Solvation in Supercritical Fluids: Its Effects on Energy Transfer and Chemical Reactions

Okitsugu Kajimoto

Department of Chemistry, Graduate School of Science, Kyoto University, Kyoto 606-8502, Japan

Received June 11, 1998 (Revised Manuscript Received September 28, 1998)

Contents

I. Introduction

In 1869, Thomas Andrews[1] first recognized the presence of the critical point, which gave birth to a new world of critical phenomena and supercritical fluid science. Later in 1879, Hannay and Hogarth[2,3] measured the solubility of solid in supercritical fluid. In 1895, Villard[4,5] attempted to observe the changes in the color of I_2 dissolved in CO_2 when CO_2 passed through the critical point. These are the pioneering works opened up the subsequent research of solubility and the microscopic observation of solvation in supercritical fluids. In 1937, Michels et al.[6] made precise measurements of the state of CO_2 near the critical point, which is still referenced in many text books for demonstrating the critical behavior of substances. In 1950s, the solubility of dense gases was a lively topic both from the scientific and technological points of view. Since then, detailed data on solubility and thermodynamic quantities of high density gases including supercritical water have been accumulated mainly from the practical interests of chemical engineering. Physical chemists have been rather indifferent to compressed dense gases except for those who were interested in high-pressure chemistry.

Since 1980s several reviews on the spectroscopy and reactions in supercritical fluids have been published both from the scientific and engineering viewpoints. Two important and pioneering reviews were published by Troe's group[7,8] in which they discussed the theoretical and experimental aspects of photodissociation, recombination, and isomerization reactions in the gas−liquid transition region. Then, researchers in the field of chemical engineering made an appreciable contribution to develop the physical chemistry of supercritical fluid. An ACS Symposium Series volume (no. 406, Supercritical Fluid Science

10.1021/cr970031l CCC: $35.00
Published on Web 01/13/1999

Professor Okitsugu Kajimoto received his B.S. and M.S. degrees from Kyoto University and then completed his Ph.D. at Osaka University under the direction of Takayuki Feuno. At Osaka University, he studied elementary gas-phase reactions and energy transfer at high temperatures with shock tube technique. He then worked with Robert Cvetanovic at National Research Council of Canada on the reactions of electronically excited species. In 1981, he moved to the University of Tokyo as Associated Professor and started the study of intracluster reactions using supersonic jet technique. He then joined the Graduate School of Science at Kyoto University as Professor of Chemistry. His current interests lie in the reactions and energy transfer in supercritical fluids and he is named as the project head of "Reactions in supercritical fluids" sponsored by Japan Science and Technology Corporation.

and Technology) published in 1989[9] compiled many excellent articles reviewing the field by that time. In particular, first four reviews following the overview by Johnston are closely related to the present review. Two subsequent ACS Symposium Series volumes (no. 488 edited by Bright and McNally and no. 514 edited by Koran and Brennecke)[10,11] also consist of reviews of the related topics. A recent review by Savage et al.[12] is rather comprehensive and includes a large number of reactions related to chemical engineering applications. Another review appeared recently in *The Journal of Physical Chemistry B* stresses the effects of inhomogeneity on the solute dynamics in supercritical fluids.[13]

The present review intends to summarize the studies of simple reactions which are important for clarifying the significance of static and dynamic solvent structure in the dynamic processes in supercritical fluids. To gain insights into the reactions taking place in supercritical fluids, one should first know the characteristics of supercritical fluids, in particular, near the critical point. The key characteristics of supercritical fluids are the inhomogeneity in space and the fluctuation in time. When a solute molecule with attractive solute−solvent interaction is placed in a supercritical fluid near the critical point, fluid solvent molecules quickly gather around the solute molecule due to the solute−solvent attractive interaction. The inhomogeneity thus caused in supercritical fluids is quite pronounced as compared with that in ordinary liquids. This process is often called "solvation" or "clustering". It is also called "density augmentation" or "enhanced local composition". The definitions of these terms are rather ambiguous. In the present review, the attention is focused on the effect of the solvent molecules in the immediate vicinity on the energy transfer and chemical reactions of the solute molecule. Therefore, the term "*solvation*" is better than clustering because clustering sometimes implies the gathering of an enormous number of solvent molecules around the solute molecule. When the term *clustering* is used in this review, it means the enhancement of solvent density within first two or three solvation shells. Such a group of molecules consisting of a solute molecule and solvent molecules in the nearby solvation shells is called a *cluster*. Although the fluctuation in the solvation structure with time has attracted less attention so far, the coupling of such fluctuation with dynamic processes in supercritical fluids will be an attractive target of the future research.

After providing theoretical and experimental backgrounds of the solvation in supercritical fluids in section II, I would like to show in section III how this solvation affects reaction dynamics in supercritical fluids and why physical chemists are so interested in studying the effects of the solvation on chemical reactions and energy transfer processes. The fundamental theories underlying each type of reaction are briefly summarized in the first part of each section in order to recognize the merit of studying a given reaction under supercritical fluid conditions. The significance and the nature of the effect that the solvation exerts on the dynamics is depending on the character of the reaction considered. This is the reason a variety of reactions have been studied in supercritical fluids.

II. Solvation in Supercritical Fluids

A. Thermodynamic Quantities in Terms of Microscopic Molecular Interactions

In the formalism of thermodynamics, all the important thermodynamic quantities can be derived from Helmholtz free energy A[14] and, therefore, the key to analyzing the supercritical solution is to evaluate Helmholtz free energy of binary mixtures with specific molecular interactions:

$$A = -k_B T \ln Q \tag{1}$$

$$Q = \frac{Z_N}{N!\Lambda^{3N}} = \frac{1}{N!\Lambda^{3N}} \int \ldots \int e^{-\beta U_N(\boldsymbol{r}_1,\boldsymbol{r}_2,\ldots,\boldsymbol{r}_N)} \, d\boldsymbol{r}_1 \ldots d\boldsymbol{r}_N \tag{2}$$

where Q is the partition function for a canonical ensemble of N particles locating at $\{\boldsymbol{r}_1,\boldsymbol{r}_2,\ldots\boldsymbol{r}_N\}$, and Λ expresses the reciprocal of the one-dimensional translational partition function, $h/(2\pi m k_B T)^{1/2}$. k_B is the Boltzmann constant and β depicts $1/(k_B T)$. U_N means the potential energy of the system consisting of N particles.

If we assume that the potential energy of the N-body system is pairwise additive as

$$U_N = \sum_{i>j} u_{ij}(r_{ij}) \tag{3}$$

the distribution function $g^{(2)}(\boldsymbol{r}_1,\boldsymbol{r}_2)$ plays an important role connecting the microscopic intermolecular

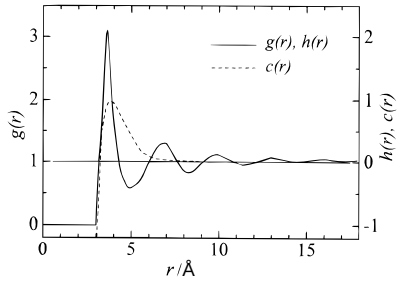

Figure 1. Typical shapes of the radial distribution function $g_{12}(r)$ and the direct correlation function $c_{12}(r)$ for a fluid. $h_{12}(r)$ is defined as $g_{12}(r) - 1$.

potential $u_{12}(r)$ and thermodynamic quantities. $g^{(2)}(\boldsymbol{r}_1,\boldsymbol{r}_2)$ is proportional to the probability of finding molecules 1 and 2 at $\boldsymbol{r}_1$ and $\boldsymbol{r}_2$, respectively. For spherically homogeneous distribution, $g^{(2)}(\boldsymbol{r}_1,\boldsymbol{r}_2)$ simply expresses the distribution of the relative distance between molecules 1 and 2, and only the function of the distance, $r = |\boldsymbol{r}_2 - \boldsymbol{r}_1|$. Hereafter, therefore, $g^{(2)}(\boldsymbol{r}_1,\boldsymbol{r}_2)$ is written as $g(r)$. A schematic shape of $g(r)$ is shown in Figure 1. Within the hard-sphere diameter, the second molecule cannot be placed and $g(r)$ is zero. Then, due to the packing structure of molecules in fluid or dense gas, a peak appears around the minimum of the interaction potential, followed by alternating valleys and peaks. In case of solid, the periodic location of molecules makes the oscillation last for a considerable length. In contrast, for liquid or dense gas, the oscillation disappears quickly, approaching the random distribution of the second molecule, i.e., $g(r) \rightarrow 1$.

With the radial distribution function $g(r)$, the potential energy of the N-body system can be expressed as[14]since

$$\bar{U} = \frac{\int\ldots\int U \mathrm{e}^{-\beta U_N}\,\mathrm{d}\boldsymbol{r}_1\ldots\mathrm{d}\boldsymbol{r}_N}{Z_N} \tag{4}$$

$$= \frac{N(N-1)}{2Z_N}\int\ldots\int \mathrm{e}^{-\beta U_N} u_{12}(r)\,\mathrm{d}\boldsymbol{r}_1\ldots\mathrm{d}\boldsymbol{r}_N$$

$$= \frac{N^2}{2V}\int_\infty^0 u_{12}(r) g(r) 4\pi r^2 \mathrm{d}r\,, \tag{5}$$

since

$$g(r) = \left(\frac{V}{N}\right)^2 N(N-1)\frac{\int\ldots\int \mathrm{e}^{-\beta U_N}\,\mathrm{d}\boldsymbol{r}_3\ldots\mathrm{d}\boldsymbol{r}_N}{Z_N} \tag{6}$$

Similarly, pressure p and chemical potential μ can be expressed in terms of $g(r)$ as

$$\frac{p}{kT} = \rho - \frac{\rho^2}{6kT}\int_0^\infty r u'(r) g(r) 4\pi r^2\,\mathrm{d}r \tag{7}$$

and

$$\frac{\mu}{kT} = \ln\rho\Lambda^3 + \frac{\rho}{kT}\int_0^1\int_0^\infty u(r) g(r;\xi) 4\pi r^2\,\mathrm{d}r\,\mathrm{d}\xi \tag{8}$$

where ξ is a Kirkwood coupling parameter expressing the variable interaction between the central molecule 1 and the other molecules in the system.[14]

Once the thermodynamic quantities are evaluated in terms of the intermolecular potential, one can derive all the important characters of liquids and dense gases such as the $P-V-T$ relation, partial molar volumes and solubility even near the critical region. However, it is not easy to evaluate $g(r)$ for dense fluids with a variety of interaction potentials. Three types of approaches have been attempted at this stage to confront this difficulty: solving integral equation, performing molecular dynamics (MD) calculations, and replacing $g(r)$ with a much simpler function or empirical parameters. In the first strategy, one needs to solve an integral equation like the Kirkwood equation[14] to obtain $g(r)$. More often, the Percus−Yevick (PY)[15] or the hypernetted chain (HNC)[16] equation with the Ornstein−Zernike procedure[17] has been used in combination with the numerical integration method. This method is, however, not easy to apply to a variety of solvent−solute systems used in actual experimental studies. The molecular dynamics calculations, the second approach, are rather easy to handle once the intermolecular potential parameters are given. However, because of its nature, the MD computations are quite time-consuming when one tries to evaluate thermodynamic quantities accurately in various conditions.

The third approach is practical and convenient for estimating thermodynamic quantities of many binary systems actually used in chemical engineering. Therefore, a variety of methods along this line have been developed in the field of chemical engineering. One example is the local composition model. Since the attractive potential $u_{12}(r)$ causes the enhanced local concentration of molecule 2, the thermodynamic quantities can approximately be expressed in terms of the *local composition* in place of the radial distribution function. Such treatment was first proposed by Wilson[18] and developed by Mollerup,[19] Prausnitz and co-workers,[20−22] and other groups. Johnston[23] extended this treatment to the mixtures in the critical region. The appropriateness of the simplified treatment has been evaluated by comparing the enhancement of local composition and relevant thermodynamic quantities with those obtained by Monte Carlo (MC) and molecular dynamic (MD) calculations[24] of the same binary mixtures. The concept of cluster stems from the local composition approximation to the radial distribution function.

B. The Cluster Concept

1. Solubility and Partial Molar Volume

One of the hot topics in Faraday Discussions held in 1953[25] was the solubility of solids in dense gases.[26] Ewald et al.[27] proposed an equation for the solubility of solids at medium-density gas as

$$\ln\left(\frac{x_2}{x_2^0}\right) = (V_2^S - 2B_{12})\frac{1}{V} + \left(V_2^S B_{11} - \frac{3}{2}C_{112}\right)\frac{1}{V^2} + \left(V_2^S C_{111} - \frac{4}{3}D_{1112}\right)\frac{1}{V^3} + \ldots \tag{9}$$

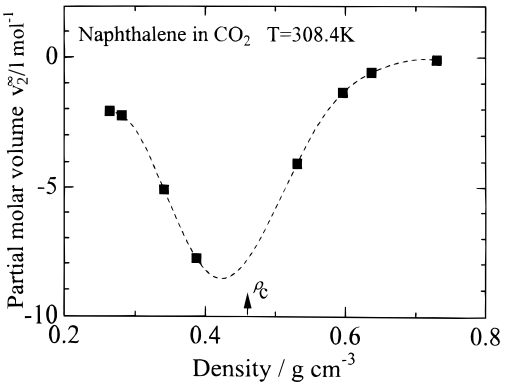

Figure 2. Partial molar volume of naphthalene dissolved in supercritical CO_2 at 308.4 K as a function of fluid density. The plot is based on the data by Eckert et al. (ref 32).

where x_2 and x_2^0 are the mole fractions of the solute 2 with and without gas molecules 1, respectively. V_2^S and V expresses the molar volume of the solid solute and the solvent gas, respectively. B_{12} denotes the second mutual virial coefficient reflecting the interaction between the solute vapor and the solvent gas, and is expressed by using the interaction potential u_{12} as

$$B_{12} = \frac{1}{2}\int_0^\infty [1 - \exp(-\beta u_{12})]4\pi r^2 \, dr \qquad (10)$$

C_{ijk} and D_{ijkl} are respective virial coefficients. They interpreted eq 9 by describing that "this excess solubility may be expressed in terms of a virial expansion in which the successive coefficients represent the *clustering* of simple gas molecules, pair of gas molecules, etc., around one molecule of solute". Franck[28] further extend the idea to consider the association equilibria between one solute and n solvent gas molecules and succeeded in reproducing the solubility curve such as naphthalene in ethylene,[29,30] benzene in N_2 and so on.

On the basis of the measured partial molar volumes of naphthalene in CO_2 and ethylene in the critical region,[31] Eckert proposed the concept of cluster of solvent molecules around the solute molecule for an intuitive understanding of large negative partial molar volume as shown in Figure 2. They also have demonstrate that the simple treatment of complexation equilibria

$$\text{solute} + n\ \text{solvent} \rightleftharpoons \text{solute(solvent)}_n$$

just like that proposed by Franck, can roughly reproduce the pressure dependence of the partial molar volume when n is assumed to be 10−50.[31,32]

Kim and Johnston[33] tried to combined such a cluster concept with the local composition model by comparing the solubility data with solvatochromism in supercritical solutions. On the basis of the MD calculations, Debenedetti[34−36] suggested that the clustering of supercritical solvent molecules could be related to the large negative partial molar volume. However, Economou and Donohue[37] argued that the mean field theory can well reproduce the partial molar volume and the cluster need not be considered. Although they admitted the local enhancement of the solvent molecules as demonstrated by the solvatochromism, they considered neither the large solubility change nor the negative molar volume to be the consequence of this enhancement around the solute. Fernandez-Prini[38] also examined the solubility in near-critical region and pointed out that the existence of cluster is not necessary to explain the observed behavior.

2. Spectroscopic Detection of Clusters

In 1980s, the spectroscopic evidences for the enhanced solvent composition around a solute were reported successively from several laboratories and now the presence of such an enhanced local composition or clustering seems to be established. As suggested in the preceding section, however, such clustering does not necessarily explain all the important phenomena observed in supercritical solutions. In this chapter the spectroscopic evidences for the solvation in supercritical fluid solutions will be discussed briefly. The readers may find more comprehensive collection of the evidences in a review of this same volume written by Tucker. An excellent review for the works in 1980s was given by Johnston.[39]

a. Spectral Shifts in Absorption Spectra. Organic physical chemistry has a long history in parametrization of reactivities for a variety of reactions occurring in organic and inorganic solvents. The reactivity is controlled by the reactant electronic nature as well as the environment where the reaction proceeds. The Hammett σ parameter[40] and its variation express the controlling factor in the reactant side whereas Y,[41] Ω,[42] Z,[43] $E_T(30)$[44] and Kamlet−Taft π^* [45,46] values express the factors in the solvent side. For example, the $E_T(30)$ value expresses the solvent polarity by using the $S_0 \rightarrow S_1$ electronic transition energy of betaine. Since the ground and excited states of betaine are ionic and neutral, respectively, polar environment stabilizes the ground state and consequently giving a blue shift in the absorption spectrum. Therefore, the larger the E_T value, the greater the polarity of the solvent.

Hyatt[47] first determined the $E_T(30)$ value of liquid and supercritical (SC) CO_2 and compared the value (34 kcal/mol) with other liquid solvent, 30.9 for *n*-hexane and 46.0 for acetonitrile. Sigman et al.[48] then examines the density dependence of the solvent parameter π^* for supercritical CO_2. They observed a large variation of π^* with varying density, though the π^* value for liquid CO_2 is almost similar to that of SC CO_2 at the same density. Yonker et al.[49,50] also determined the π^* parameters for supercritical CO_2, N_2O, CCl_3F, NH_3 Xe, SF_6, and CO_2-CH_4 mixtures.

Kim and Johnston[51] first tried to use the bathochromic shift of absorption spectra, E_T, as a measure of the local solvent density. They measured the density dependence of the E_T value of phenol blue in ethylene, CF_3H, and CF_3Cl, and found that the E_T value at low density was smaller than that predicted by the second-order quantum mechanical perturbation theory of transition energies; the excited state of phenol blue was more stabilized than expected. This observation suggests that the local dielectric

constant around a solute molecule is larger than that of bulk fluid, indicating the occurrence of the local density enhancement. They estimated the local density near the solute molecule to be equal to the bulk density that gives the same E_T value in the theoretical prediction using the *bulk* dielectric constant of the fluid. Further, they predicted the linearity between the E_T value and the rate constant in supercritical fluid solvents, which is now established in a variety of reactions and even in energy transfer as given in the next section. Yonker and Smith[52−54] also discussed the relation between the π^* value and the local solvent density in terms of a dielectric continuum model.

b. Stokes Shift in Fluorescence. When a molecule consists of electron-donating and electron-accepting parts, the electron moves from the donor to the acceptor on photoexcitation and the molecule acquires a large dipole moment. Such reaction is called the intramolecular charge transfer reaction and known to be quite sensitive to the solvent polarity. The fluorescence emitted from the charge transfer (CT) state is largely red-shifted from the excitation wavelength because of the large stabilization of the CT state by polar solvent. Using such a spectral shift, called as a Stokes shift, one can easily evaluate the polar nature of the solvent including supercritical fluids. Kajimoto et al.[55] first applied such Stokes shifts to estimate the solvent clustering around the CT molecule in polar supercritical CF_3H. They showed that the Stokes shift of 4-(*N*,*N*-dimethylamino)benzonitrile (DMABN) in low-density CF_3H is much larger than the shift expected from simple Onsager reaction field theory (Lippert−Mataga equation) and attributed this to the local enhancement of solvent density.

Y.-P. Sun et al.[56] observed both the absorption and fluorescence spectra of DMABN and ethyl 4-(*N*,*N*-dimethylamino)benzoate (DMAEB) in supercritical CF_3H, CO_2, and ethane in a wide density range. They found that DMAEB could form the CT state even in nonpolar supercritical CO_2 due to the different excited-state potential surface from that of DMABN as is well-known in nonpolar liquid solvent. The trend in the bathochromic shifts in the absorption spectrum was found to be quite similar in both compounds. In the bathochromic shifts in the CT fluorescence spectra of DMAEB measured in CF_3H, they observed the same trend as that reported previously for DMABN.[55]

c. X-ray and Neutron Diffraction Measurements. X-ray or neutron diffraction is a powerful tool to detect the time-averaged fluctuation or the inhomogeneity in supercritical fluid. With the small-angle scattering experiment one can obtain the information on the long-range structure of the fluids, whereas the wide-angle scattering experiments provide the information on the short-range order of the fluids. Nishikawa et al.[57−59] applied this technique to supercritical CO_2 and CF_3H and estimated the radial distribution function, which is shown in Figure 3 for supercritical CO_2 at 308 K together with that of liquid CO_2. The thermodynamic parameters for the points A−E are given in Figure 4. Although the radial

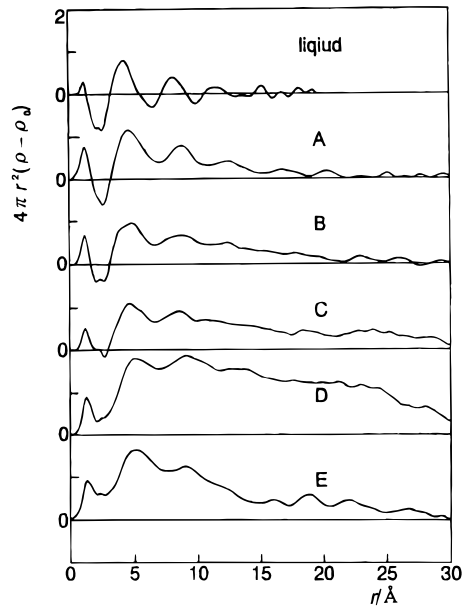

Figure 3. Radial distribution functions of liquid and supercritical CO_2 evaluated with the X-ray scattering technique. Note that the ordinate is not $g_{11}(r)$ but $4\pi r^2(g_{11}(r) - 1)$. The top plot corresponds to liquid CO_2 and other plots downward are for the states along the isotherm at 308 K; the labels A−E depict the states as defined in Figure 4. (Reprinted from ref 61. Copyright 1997 American Chemical Society.)

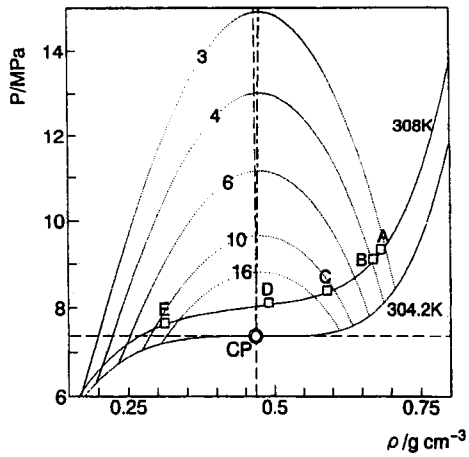

Figure 4. Line of maximum fluctuation is shown by the chain line on the $P-\rho$ diagram. The line starts from the critical point and extends upward. The fluctuation contours are also shown by dotted lines. (Reprinted from ref 61. Copyright 1997 American Chemical Society.)

distribution function of pure fluid, $g_{11}(r)$, is not necessarily the same in its behavior as $g_{12}(r)$ for a solute−solvent system, it is worthy to know how $g_{11}(r)$ changes with varying density. For liquid CO_2, the first to the third peaks are clearly seen in the range of 4−15 Å. For supercritical CO_2, these peaks are broadened and the radial distribution function takes a positive value in a wide range of radial distance. This positive region further increases as the critical region is approached and could be considered as an indication of a cluster. However, one should note that $g_{11}(r)$ shows just the average enhancement, not guaranteeing the real existence of the cluster of this size. Further, Nishikawa and Morita[60] evaluated the spatial fluctuation (inhomogeneity) from the zero-

angle X-ray scattering intensity $I(0)$ observed at various (P,V) conditions near the critical point and found that the fluctuation, $\langle(\Delta N)^2\rangle/\langle N\rangle$, showed the maximum along a line passing through the critical point on the $P-V-T$ chart[60,61] as is shown in Figure 4. They considered this line to be a kind of third-order phase transition.

Ishii et al.,[62−64] using the neutron diffraction technique, evaluated the radial distribution function and the correlation length, a measure of the fluctuation, along an isotherm. For supercritical Xe, CO_2, and CF_3H, they showed that the fluctuation became maximum at the critical density and the coordination number was a linear function of the reduced density.

C. Applicability of the Cluster Concept to Phenomena in Supercritical Fluids

Cluster is a simple and practical concept to explain a variety of phenomena in supercritical fluids. However, one should be cautioned not to abuse this concept. In the present section, the usefulness and limitation of the cluster concept will be discussed from the three viewpoints. First one is the spatial range of the phenomena of interest, i.e., the short-range or long-range phenomena. The second one is the nature of interaction which governs the specific phenomenon, the attractive or repulsive interaction. The final viewpoint concerns the fluctuation. The important features of supercritical fluids is its large fluctuation of density both in space and in time, which may control the phenomena occurring in supercritical state, particularly near the critical point.

1. Short-Range or Long-Range Phenomena

Supercritical fluids have been studied in many aspects including the equation of state, partial molar volume, compressibility, heat conductivity, solubility, diffusion, and viscosity, in addition to spectroscopy and chemical reactions. To classify these properties in terms of their fundamental molecular interactions, several viewpoints are proposed: microscopic or macroscopic properties, short-range or long-range interactions, and direct or indirect interactions. Although these viewpoints are similar, the details are different and sometimes the difference among these viewpoints are ambiguous.

a. Macroscopic or Microscopic. The classification by the term "macroscopic" or "microscopic" is rather ambiguous. Table 1 represents the hierarchy of properties of supercritical fluids or solutions in the rough order of increasing microscopic character. The quantities appearing in the upper part of the table are usually obtained by means of macroscopic or bulk measurements. On the other hand, the quantities in the lower part are evaluated mainly by spectroscopic methods which detect microscopic molecular interactions acting within a few angstroms. Technique of measuring the properties could be used as a part of definition. The characteristic length necessary for the property to appear would be a more quantitative measure to differentiate macroscopic properties from microscopic ones. Among the thermodynamic quantities in Table 1, some are closely related to the solvation or clustering while others are rather insensitive to it. The macroscopic properties in the upper part of Table 1 are usually not greatly affected by the solvation. The property of solvent fluid mostly characterizes the features; the solute molecules give just a perturbation. On the other hand, the lower part of Table 1 lists the solute properties in supercritical fluids, which directly reflect the solvation structure in the vicinity of the solute.

Table 1. Hierarchy in the Properties of Supercritical Fluid in the Order of Increasing Microscopic Character

Phenomena		Detection	Theory
Static	Dynamic		
	<Macroscopic>		
P-V-T	Convection	P-V-T	Thermodynamics
Isothermal compressibility	Thermal conductivity		
Partial molar volume	Diffusion		
Solubility	Viscosity	X-ray, Neutron scattering	$g(r)$
Spectral shift	Energy transfer	IR, Raman	Local Composition
	Reaction	UV absorption	Clustering
		NMR, ESR	
		ps, fs-measurements	MC, MD
	<Microscopic>		

b. Short-Range or Long-Range. The term "short-range" or "long-range" expresses the characteristic length or diameter of the area where a static or dynamic phenomenon of interest takes place. For example, the isothermal compressibility expresses the gathering of an enormous number of solvent molecules and the range of gathering molecules is quite long. On the other hand, solvation or clustering ordinarily indicates the gathering of the solvent molecules within a few angstroms and can be classified as a short-range phenomenon. The phenomena discussed in the present review are spectral shifts, energy transfer, and reactions, all of which belong to short-range category and are closely related to the clustering. The width of the solvation shell could be used for a measure of the cluster; for instance, a solute molecule and the solvent molecules within a certain solute−solvent distance can be considered to constitute a cluster. In a simple model of clusters, the number of solvent molecules in the first solvation shell is the important parameter controlling the short-range phenomena. In terms of the radial distribution function, the number of solvating molecules could be estimated by integrating $g(r)$ in the range of the first solvation shell.

c. Direct or Indirect. According to the Ornstein−Zernike relation:

$$h(r_{12}) = c(r_{12}) + \rho\int c(r_{13})[g(r_{23}) - 1]\,\mathrm{d}\boldsymbol{r}_3 \quad (11)$$

$h(r_{12})$ ($\equiv g(r_{23}) - 1$) consists of the two contributions, direct and indirect. The direct contribution, expressed by the direct correlation function $c(r_{12})$, represents the direct interaction between the solute 1 and the solvent molecule 2 *in the fluid* and could be approximated by $\exp(-u_{12}(r)/kT) - 1$ in the $\rho \to 0$ limit. The second term of eq 11 represents the indirect contribution, which is the sum of all the contributions $c(r_{13})$ from the solvent molecules 3 being present around the molecule 2 with the weight of

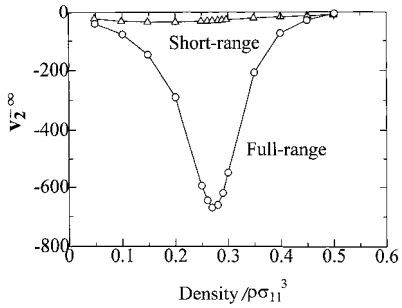

Figure 5. Partial molar volume of pyrene, evaluated from PY calculations, in supercritical CO_2 at $T_r = 1.02$ as a function of CO_2 density. The contribution from the short-range direct term is negligibly small. All quantities are reduced in terms of solvent's Lennard-Jones parameters. The plot is based on the data by Chialvo and Cummings (ref 65).

$\rho(g(r_{23}) - 1)$. To illustrate these interactions, one can imagine that the molecule 2 wears clothes. Then, the direct part $c(r_{12})$ expresses the radial distribution of the molecule 2 determined by the interaction between the solute molecule 1 and the solvent molecule 2 without the clothes. On the other hand the indirect part means the effect of the clothes on the distribution of molecule 2; if the clothes are very thick and rough, they disfavor the presence of the molecule 2 in close vicinity of the molecule 1.

As shown in Figure 1, $c(r_{12})$ is a monotonic function of r_{12}. It decays monotonically to zero with increasing r_{12} after passing the maximum. On the other hand, $g(r) - 1(\equiv h(r))$ shows an oscillation in its tail. Therefore, the second term of eq 11, the indirect term, is responsible for this oscillating tail. Since the indirect term is proportional to the bulk density, the oscillatory features are enhanced at high densities such as pure liquid state. Thus, the density or the number of solvent molecules in the first solvation shell is determined by the two factors, $c(r_{12})$ and the indirect term. The contribution of $c(r_{12})$ is usually much larger than the indirect term. Roughly speaking, the *short-range* phenomena are controlled by the *direct* contribution $c(r_{12})$.

Using the above concept, Chialvo and Cummings[65] evaluated the direct and indirect contributions separately in various thermodynamic quantities such as partial molar volumes, isothermal compressibility, and residual chemical potentials of the system consisting of a solute pyrene and solvent CO_2 molecules. They have demonstrated that the partial molar volume and isothermal compressibility are determined by the indirect contribution whereas the residual chemical potential is controlled by the direct contribution. Figure 5 shows the partial molar volume of pyrene in supercritical CO_2 as a function of CO_2 density, together with the contribution, from the short-range term. Apparently, the contribution from the short-range term is negligibly small in all the density range and the negative partial molar volume around the critical density should be attributed to the large compressibility of the solvent itself in that region. That is, the long-range, indirect contribution determines the features of the partial molar volume.

Munoz and Chimowitz[66] examined the controlling factor of the chemical potential, which relates to solubility, in near-critical fluid using integral equation calculations. They noticed that the chemical potential was relatively invariant to the local density enhancement because of countermanding energetic and entropic effects. Their analysis showed that although the observed solvation gave an appreciable enthalpy gain to enhance the solubility, the entropy loss due to the gathering of solvent molecules disfavored the solubility. Their findings suggest that we must take the total thermodynamic balance of the system into account to discuss the thermodynamic quantities of supercritical solutions. It should be noted, however, that for strongly interacting systems such as ions in supercritical water, the chemical potential is significantly influenced by the local density enhancement.

d. Clustering Number and the Direct Contribution. The above arguments led to the conclusion that the concept of cluster should be applied only to the properties reflecting the character of molecular dimensions, i.e., short-range phenomena. For the energy transfer and chemical reactions the short-range interactions play a critical role and the concept of cluster acts as an useful measure. For the phenomena given in the lower part of Table 1, one can develop the discussion based on the solvation or clustering number of solvent molecules around a solute.

The clustering number N_{clus} can be estimated by integrating the radial distribution function within an appropriate range, r_1 to r_2, which defines the solvation shell. As given in eq 12 and Figure 6, we candivide the contributions to N_{clus} into two parts, $N_{clus}^{(1)}$ and $N_{clus}^{(2)}$:

$$\begin{aligned} N_{clus} &= 4\pi\rho\int_{r_1}^{r_2} g_{12}(r) r^2\, dr \\ &= 4\pi\rho\int_{r_1}^{r_2} (1 + h_{12}(r)) r^2\, dr \\ &= N_{clus}^{(1)} + N_{clus}^{(2)} \qquad (12) \\ N_{clus}^{(1)} &= 4\pi\rho\int_{r_1}^{r_2} r^2\, dr \\ N_{clus}^{(2)} &= 4\pi\rho\int_{r_1}^{r_2} h_{12}(r) r^2\, dr \cong 4\pi\rho\int_{r_1}^{r_2} c_{12}(r) r^2\, dr \end{aligned}$$

The first contribution $N_{clus}^{(1)}$ simply corresponds to the volume of the solvation shell multiplied by the *bulk* fluid density and equals to the average number of solvent molecules in this volume. It increases linearly with increasing bulk density as is shown in Figure 6. The second contribution $N_{clus}^{(2)}$ equals to the integration of $h_{12}(r)$ within the solvation shell and represents an increment of the solvent molecules due to the local molecular interactions. After passing the maximum around the critical density, $N_{clus}^{(2)}$ decreases with increasing fluid density due to the solvent−solvent repulsion. Since the main contribution to $h_{12}(r)$ at the short distance comes from the direct correlation function $c_{12}(r)$, $N_{clus}^{(2)}$ could be approximated by the integration of $c_{12}(r)$ instead of

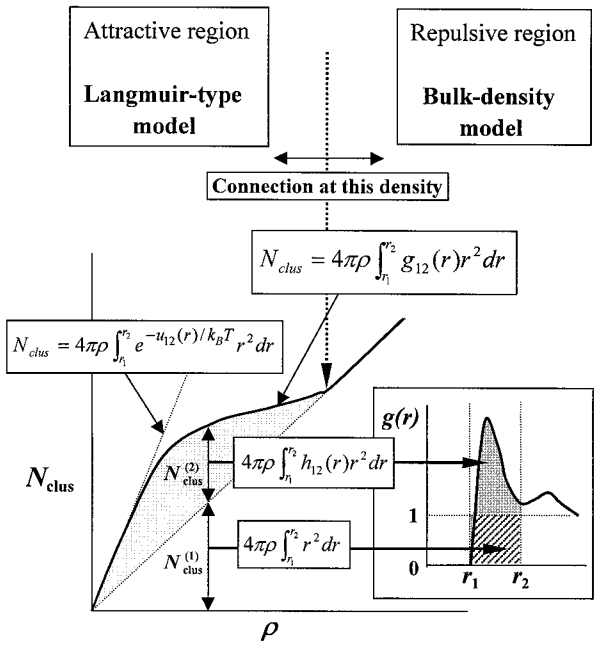

Figure 6. Clustering number derived from the radial distribution function $g_{12}(r)$ can be divided into two components $N^{(1)}_{clus}$ and $N^{(2)}_{clus}$. The density dependences of $N^{(1)}_{clus}$ and $N^{(2)}_{clus}$ are schematically illustrated. In the low-density region, attractive interaction plays a significant role and hence $N^{(2)}_{clus}$ gives a considerable contribution. In the high-density region, however, $N^{(1)}_{clus}$ becomes the main component.

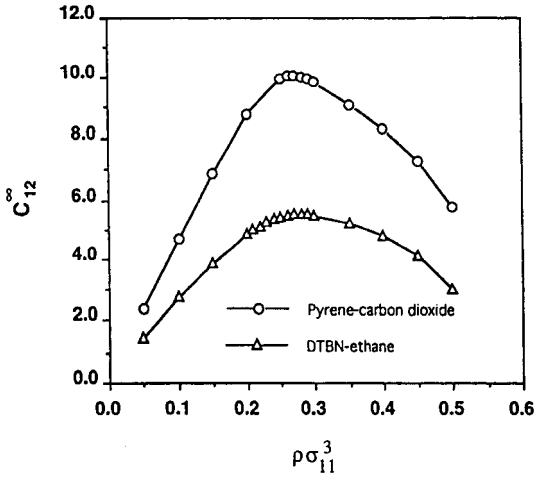

Figure 7. Plot of C^{∞}_{12} as a function of bulk density for the pyrene−CO_2 and the DTBN−ethane systems calculated by Chialvo and Cummings. (Reprinted with permission from ref 65. Copyright 1994 American Institute of Chemical Engineering.)

$h_{12}(r)$ in the range of r_1 to r_2. The behavior of this integral must be parallel to that of the direct correlation function integral C^{∞}_{12}

$$C^{\infty}12 = 4\pi\rho\int_0^{\infty} c_{12}(r) r^2 \, dr \qquad (13)$$

because $c_{12}(r)$ is small outside the range of r_1 to r_2. Figure 7 shows the plot of C^{∞}_{12} as a function of bulk density for the pyrene−CO_2 system calculated by Chialvo and Cummings.[65] In the low-density region, C_{12} increases linearly to the fluid density, passes the maximum, and then decreases with increasing density. This behavior is caused by the negative value of $c(r_{12})$ at small r_{12}, which becomes prominent at high densities.

On the basis of the density dependence of each component, $N^{(1)}_{clus}$ and $N^{(2)}_{clus}$, one can understand the behavior of the clustering number N_{clus} with varying fluid density. As depicted schematically in Figure 6, it increases linearly at low densities but more rapidly than expected from the increase of the bulk density when the molecular interaction $u_{12}(r)$ attracts solvent molecules toward the solute. In the medium-density region, the contribution by the attractive interaction $N^{(2)}_{clus}$ decreases gradually, and at high densities the total clustering number finally merges to the simple density contribution $N^{(1)}_{clus}$. Such a behavior of N_{clus} provides a basis for the Langmuir-type adsorption model of solvation which will be discussed in section II.D.

2. Attractive or Repulsive Compression

In various phenomena occurring in supercritical fluids a plateau is often observed around the critical density when the observed quantity is plotted against the fluid density. One example from the pioneering study by Simmons and Mason[67] is given in Figure 8. The rate of the dimerization of CF_2=CFCl showed a plateau just around the critical density. Sun et al.[56] showed that the bathochromic shift in the absorption and fluorescence spectra of DMABN and DMAEB gave a similar trend. The recent measurements of the energy transfer and spectral shifts reported from Fayer's group[68,69] provide us another example, which will be discussed in section III. A.

At low supercritical fluid densities, the attractive force is the driving force for the cluster formation.

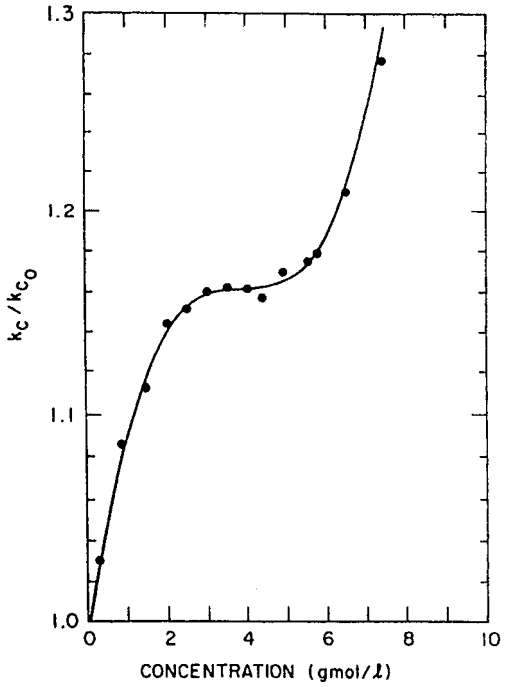

Figure 8. Rate constant for the dimerization of CF_2=CFCl as a function of reactant density at 135 °C. A plateau is observed around the critical density. (Reprinted with permission from ref 67. Copyright 1972 Elsevier Science.)

When the kinetic energy of fluid molecules is smaller than the solute−solvent attractive potential, the solvent molecules tend to gather around the solute molecules to form a cluster. The number of clustering solvent molecules increases with increasing fluid density up to around the critical density and then levels off toward the solvation number in the liquid phase, as was shown in the preceding section. The plateau observed in various experiments most probably has its origin in the leveling off or the saturation in the solvation number, because such a plateau has been observed for the short-range phenomena.

When the density is further increased in excess of the liquid density, the repulsive interaction comes into play. The repulsive compression then increases the number of solvent molecules in the solvation shell. Although the repulsive interaction disfavors the enthalpy of the solvent system, the electronic perturbation from the surrounding solvent molecules may be intensified. Consequently, the red shift of the electronic spectrum and the rate of chemical reactions again start increasing with increasing density. It is important to recognize that the driving force is different in different density regions; the attractive interaction is predominant in the low-density region while the repulsive interaction controls the phenomena at high densities.

3. Fluctuation

a. The Features of Fluctuation Revealed by MD Calculations. As is well-known, the salient features of the supercritical fluid is "fluctuation" in space and time. Although various phenomena can be explained in terms of the average clustering number $\langle n \rangle$, the important variables of supercritical fluids are the space fluctuation of the clustering number $\langle (\Delta n)^2 \rangle$ and the time-dependent fluctuation of n, $\langle \Delta n(0) \Delta n(t) \rangle$. No definite experimental results showing the effect of these fluctuations on energy transfer or reactions have reported so far. A simple molecular dynamics (MD) simulation was performed to illustrate these fluctuations. A spherical solute atom of large attractive L-J potential was immersed in spherical solvent atoms modeling Ar.[70] The solvent atoms within 5 Å of the solute atom was considered to form a cluster and the solvation number was estimated. The average clustering number, the cluster size distribution, and the time-dependent variation of the cluster size were evaluated.

Figure 9 illustrates the density dependence of the cluster size distribution evaluated from the above-mentioned simulations. The distribution is widest at the critical density. When the simulation is performed close to the critical conditions, the cluster size distribution becomes much wider. Using small-angle X-ray scattering, Nishikawa et al.[60,61] showed that the extremum of $\langle (\Delta n)^2 \rangle$ exists along the extension of the coexistence curve of gas and liquid in the $P-T$ phase diagram of pure CO_2 and CF_3H solvents. We can expect that the fluctuation of solvation number or the size distribution also shows extremum on the same curve. The effects of the wide size distribution on the reaction and energy transfer, if any, would become maximum along this line.

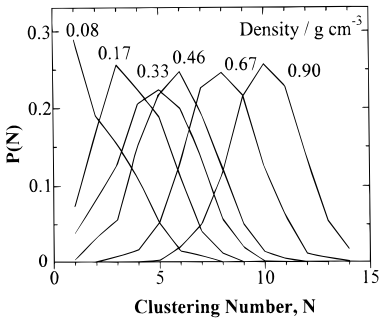

Figure 9. Density dependence of the cluster size distribution based on a MD simulation (see text). The size distribution is widest at the critical density. (Reprinted with permission from ref 70. Copyright 1997 Deutsche Bunsen Gesellschaft fur Physikalische Chemie.)

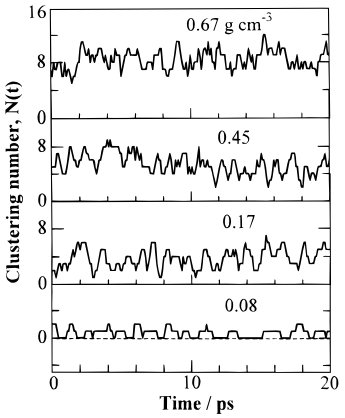

Figure 10. Time-dependent fluctuation of the solvation number based on a MD calculation (see text).

The time-dependent fluctuation of the solvation number is shown in Figure 10 based on the MD calculations. Although the detailed features of the fluctuation varies with the fluid density, the characteristic time of the fluctuation seems to be about 1 ps. When the transition state is sensitive to the environment, the instantaneous barrier height of the reaction may fluctuate with this time scale. If the rate of barrier crossing is of the same order to the fluctuation, the rate would be significantly affected due to the fluctuating barrier height. We have conducted the electron-transfer reaction of *N*,*N*-dimethylbenzonitrile in supercritical CF_3H to detect the effect of time-dependent environmental fluctuation. Unfortunately, no definite clue of the interference between the environmental fluctuation and the barrier crossing rate have been recorded thus far. Nevertheless, such experiments is extremely interesting to clarify the interplay between fluctuation and reaction dynamics.

b. Temperature-Dependent Features of Clusters. The characteristics of clusters varies with temperature as schematically shown in Figure 11. Near the critical point at $T \approx T_c$, the solvent fluid molecules themselves are apt to form clusters of extremely large size, which change their shape and range with time. When solute is dissolved into the fluid under such conditions, the solute molecule is ordinarily accommodated within a large clusters and probably makes the cluster lifetime longer due to the stabilization by attractive interaction. Thus, the

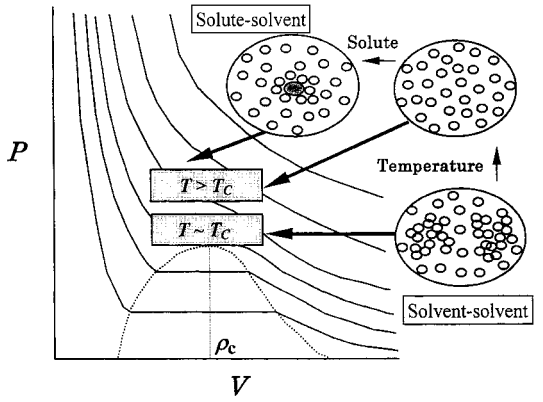

Figure 11. Different character of clusters formed in different temperature ranges. Near the critical temperature the solvent molecules tend to form a large cluster even without a solute molecule. At higher temperatures, the solute molecule with strong attractive interaction is necessary to trigger the clustering of solvent molecules.

lifetime of the polar environment for the solute molecule becomes longer as the critical point is approached. In addition, if the solute molecule is located near the center of the solvent cluster, the polarity fluctuation should be small, just like in the liquid.

At the temperatures appreciably higher than the critical temperature $T > T_c$ ($T_r \geq 1.05$), the solvent fluid itself is rather uniform and homogeneous as depicted in the figure, and the isothermal compressibility of the fluid is not large. However, when a solute with large attractive solute−solvent interaction is placed in this fluid, the solvent molecules form a cluster surrounding the solute molecule. The number of solvent molecules participating in the cluster under such conditions are rather small and they form only the first and second solvation shells, in contrast to the above-mentioned large clusters near the critical point. The solute−solvent interaction is more important at this temperature than the solvent−solvent interaction. Depending on the balance between the solute−solvent interaction and the temperature (kinetic energy of solvent molecules), the cluster lifetime varies probably in the range of 0.5 to 2 ps. The time scale of the fluctuation in the environmental polarity will be the same order, which is much shorter than that near the critical point. In this way, by adjusting the temperature of the system, one can adjust the lifetime of the cluster and consequently the fluctuation (correlation time) of the polar environment around the solute molecule.

c. The Lifetime of Clusters. The experimental measurement of the cluster lifetime or the correlation time of the density fluctuation has not yet been conducted. Therefore, the cluster lifetime is estimated from the MD calculations. Patsche and Debenedetti[34] carried out the MD calculations of the system consisting of a Xe-like Lennard-Jones atom and Ne-like Lennard-Jones atoms in supercritical conditions. They noticed the enhancement of Ne density around the solute Xe. Figure 12 shows the time dependent location of the five Ne atoms surrounding the Xe atom at $T_r = 1.4$ and $\rho_r = 0.35$. Three Ne atoms out of five are still in the first solvation shell 2 ps after

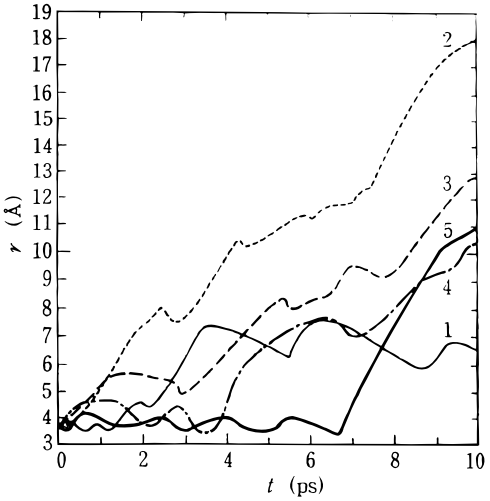

Figure 12. Time dependence of solute−solvent distance corresponding to the five closest Ne atoms (indicated as 1−5 in the figure) surrounding a Xe atom at $T_r = 1.4$ and $\rho_r = 0.35$. All Ne atoms are located within 5 Å during first 1 ps. The lifetime of clusters could be defined based on the loss of *originally* clustering solvent molecules. (Reprinted with permission from ref 34. Copyright 1989 American Institute of Physics.)

the start. If the lifetime of cluster is defined from the decay of the atoms originally surrounding the solute atom, the lifetime is estimated to be 1−2 ps in the present case. Since other Ne atoms can enter into the solvation shell while these five atoms depart from it, the actual polarity of the environment is maintained for the period much longer than the cluster lifetime defined here.

Liew et al.[71] performed the MD calculation for the pyrene−CO_2 system. They defined the cluster as consisting of a pyrene molecule and the CO_2 molecules having the radial kinetic energy less than or equal to their pair potential energy. They found that the clustering CO_2 molecules originally in the first solvation shell remained there with a lifetime of 2 ps.

In the above procedure of estimating the lifetime, replacement of solvent molecules is stressed too much. Even though the replacement takes place, the polarity of the environment does not change. Only when a solvent molecule departs from the solvation shell and no solvent molecule comes in, the polarity of the environment decreases. Therefore, the change in the number of solvating molecules is important rather than the replacement. The reaction dynamics should be related to the correlation time for the number of solvating molecules in the first solvation shell.

D. A Simple Langmuir-Type Model of Clustering

1. Basic Idea

To explain the spectral shifts observed in the absorption and fluorescence spectra, Kajimoto et al.[55,72] proposed a simple Langmuir-type model for the evaluation of actual clustering number in the first solvation shell. When the intermolecular potential between a solute and a solvent is given as $u_{12}(r)$ and the range of the first solvation shell is assumed as r_1

$- r_2$, the bulk solvent density ρ_1 which provides a single solvent molecule in the solvation shell can be evaluated in the low-density limit as

$$1 = \rho_1 \int_{r_1}^{r_2} \exp(-u_{12}(r)/kT) 4\pi r^2 \, dr \qquad (14)$$

Then, the bulk density necessary for supplying m molecules in the first solvation shell, ρ_m, would be obtained by putting m instead of 1 in eq 14. However, the first solvation shell can accommodate only a limited number of solvent molecules because of the limited surface area of the solute molecule. To express such restriction, the idea of Langmuir adsorption equilibrium is adopted. If the maximum number of molecules accommodated in the first solvation shell is n, and m molecules are presently accommodated, the Langmuir isotherm requires the equilibrium like

$$k_0 \frac{m}{n} = k_1 \left(1 - \frac{m}{n}\right) \rho \qquad (15)$$

where the left-hand side is the out-going rate with the rate constant of k_0 and the right-hand side corresponds to the in-coming rate. Using the condition that ρ becomes ρ_1 for $m = 1$, the equation becomes

$$\rho = \rho_1 \frac{m(n-1)}{n-m} \qquad (16)$$

The resulting equation expresses the relation between the number of solvating molecules m and the bulk density of the supercritical solvent ρ. By applying this equation one can estimate the solvation number at a given fluid density.

To apply this model to a specific solute−solvent combination, one has to estimate the solute−solvent intermolecular interaction potential $u_{12}(r)$ first and calculates ρ_1 according to eq 14. A simple way of obtaining the intermolecular potential is to measure the solubility of the solute into the supercritical fluid of interest. One could use absorption spectroscopy or other analytical technique to measure the concentration of solute dissolved in supercritical fluid at varying solvent density. Then, using eq 9, the mutual virial coefficient B_{12} is derived; B_{12} in turn is a function of the intermolecular potential as given in eq 10. Equation 10 can be solved easily by numerical integration with an assumed form of interaction potential. Although Kajimoto et al. used the Sutherland potential with two parameters C and σ

$$u_{12}(r) = -\frac{C}{r^6} \qquad r > \sigma \qquad (17)$$
$$= \infty \qquad r \le \sigma$$

any potential could be used.

2. Applications

Although the above model looks too simple, it turned out that this model excellently reproduces various phenomena occurring in supercritical solutions, in particular, the phenomena where the first solvation shell plays an essential role. Kajimoto et al.[72] measured the maximum of the absorption spectrum of benzonitrile (BN) as a function of fluid density and found that the observed red-shift significantly deviates from that predicted from the Onsager relation. On the basis of the spectral shift observed for 1:n BN−CF_3H complexes in a supersonic jet, they determined the spectral shift per attaching CF_3H molecule. By assuming the linear relation between the clustering number and the red-shift in supercritical fluid, they further estimated the solvation number as a function of solvent density. The clustering number thus evaluated in supercritical fluid solvent is greatly enhanced in the lower density region, gradually saturates toward high density, and approaches to the solvation number in the liquid phase. This behavior is in excellent agreement with that expected from the Langmuir adsorption isotherm. Using the measured solubility of BN in CF_3H, they estimated the intermolecular potential and calculated the solvation number as a function of fluid density by means of the Langmuir-type model. If the maximum number of solvent molecules in the first solvation shell is assumed to be 6, the estimated solvation number perfectly fits the curve obtained from the spectral shift. Recently, Bulgarevitch et al.[73] measured the absorption spectra of 4-nitroanisole in supercritical CO_2 at various fluid densities. They found that the spectral shift was well reproduced by the Langmuir-type model with the maximum number of CO_2 molecules in the first solvation shell being 8.

Nakagawa[74] showed that the ionization potential of anthracene measured in supercritical Xe as a function of Xe density can well be reproduced by using the above model. Within the framework of the Born approximation, the ionization potential should follow the relation

$$I_p = I_g + V_0 - \frac{e^2}{2R(1 - \epsilon^{-1})^{-1}} \qquad (18)$$

where I_g and V_0 are the adiabatic ionization potential in the gas phase and the energy of the conduction band for the injected electron, respectively. ϵ is the dielectric constant of the fluid as a function of bulk density. R expresses the radius of the molecule. As Figure 13 shows, this relation does not reproduce the observed trend. If one takes into account the clustering number which is estimated by the above-mentioned procedure, the observed trend was precisely reproduced by the equation

$$I_p = I_g + V_0 - n\Delta = I_g + V_0 - \Delta \frac{m\rho}{\rho_1(m-1) + \rho} \qquad (19)$$

where Δ means the polarization energy induced by association of one fluid molecule with the solute molecule and taken to be −0.18 eV for an anthracene molecule in supercritical Xe.

Schwarzer et al.[75] also applied the Langmuir-type cluster equilibrium for the analysis of vibrational energy dissipation from highly excited ground-state azulene molecule to supercritical fluid molecules

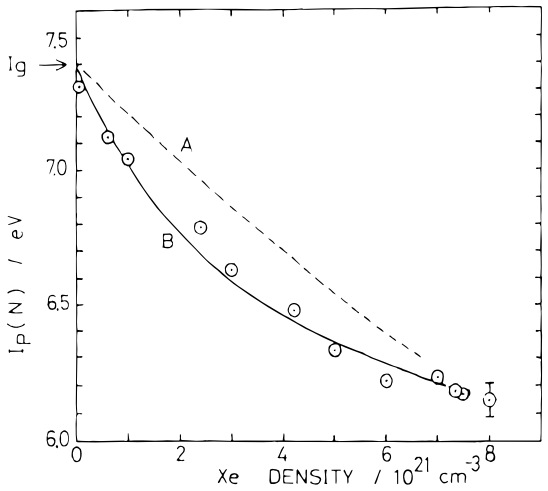

Figure 13. Ionization potential of anthracene measured in supercritical Xe as a function of Xe density: (line A) born approximation, and (line B) Langmuir-type approximation. (Reprinted with permission from ref 74. Copyright 1996 Elsevier Science).

outside. They found that the energy transfer rate would not increase linearly with increasing density of supercritical fluid and, therefore, sought the mechanism which reduces the energy transfer efficiency as the density increases. They proposed that the solvent molecules in the immediate vicinity must shield the hot molecule from direct collisions with the solvent molecules outside the solvation shell. To evaluate the shield efficiency, they estimated the clustering number using the Langmuir-type model. Although the model using the estimated solvation number explained the observed trend in the low- and medium-density region, it could not reproduce the observation at high densities, where the energy-transfer efficiency again becomes higher. The discrepancy probably suggests that the mechanism of energy dissipation at low density is different from that at high density where the heavy packing of solvent molecules may cause a different kind of energy-transfer mechanism.

Flanagin et al.[76] used the Langmuir-type model for estimating the maximum solvation number of water to various cation and anion species and found that such a simple approximation well explains the solvation in supercritical water. Using the molecular dynamic simulation−statistical perturbation method, they calculated the number of water molecules in the immediate vicinity of the anion produced during the course of the symmetric S_N2 reaction, $Cl^- + CH_3Cl \rightarrow CH_3Cl + Cl^-$. They found that the Langmuir-type model could predict the water solvation number as a function of fluid density and this solvation number correctly predicted the free energy of solvation. Furthermore, in the ion solvation in supercritical water, the density dependence of the water solvation number estimated from the model is in excellent agreement with the result of MD calculations. They evaluated the parameters of the Langmuir-type model suitable for calculating the solvation number for various alkali atom cations and halogen anions, which provide the simple way of estimating the solvation number and free energies of solvation at a variety of pressures and temperatures of supercritical water.[77]

3. An Extension

The above-mentioned model of clustering considers only the solute−solvent attractive interaction explicitly and the solvent−solvent repulsion is taken into account by assuming the Langmuir-type equilibrium. Although such a model can well express the saturation in the number of molecules in the first solvation shell with increasing density, it cannot represent the further increase of the solvating molecules at much higher bulk density. As mentioned in section II.C, at such high density, we have to take into account the effect of repulsive compression around the solute molecule. The attractive interaction controls the clustering up to slightly above the critical density. Above this density the repulsive compression controls the structure of the solvation shell. The repulsive force from the outside further increases the number of solvent molecules in the first solvation shell or it compresses the radius of the first solvation shell, making the effect of second solvation shell nonnegligible.

Equation 12 suggests us how to incorporate the effect of repulsive compression in the simple clustering model mentioned in section II.D.1. The solvation number N_{clus} is determined by the two terms in eq 12. The first term $N_{clus}^{(1)}$ increases linearly with the density while the second term, $N_{clus}^{(2)}$, increases sharply in the low density region and then levels off in the medium-density region. Both the linearly increasing term and the contribution from $N_{clus}^{(2)}$ are included in the Langmuir-type adsorption model at low and medium densities. As indicated schematically in Figure 6, $g_{12}(r)$ is approximated as $\exp(-u_{12}(r)/k_BT)$ at the low-density limit. As the density increases, this approximation fails because of the repulsive interactions between the solvent molecules, and the integration of $h_{12}(r)$ decreases rapidly above the critical density. However, even at the higher densities, $N_{clus}^{(1)}$ still increases linearly with the density. This increase is due to the repulsive compression which pushes the solvent molecules to the repulsive wall of the interaction potential. As stated in section II.C.2, the additional solvent molecules in the solvation shell could exert the electronic effects on the solute molecule or enhance the removal of the internal energy of the solute (chromophore).

To connect the N_{clus} value estimated in the attractive region to that in the repulsive region, one may calculate the fluid density that makes $N_{clus}^{(1)}$ equal to the maximum solvation number n of eq 16, by assuming $N_{clus}^{(2)} \approx 0$ at this density. One can connect the curve from the Langmuir-type model to that for the repulsive compression regime at this density, as Figure 6 indicates. However, the density thus calculated is usually too high; in the case of DMABN in supercritical CF_3H, the density corresponding to seven CF_3H molecules ($n = 7$) in the first solvation shell becomes 1.28 g/cm^3. Therefore, the range of the solvation shell can be slightly extended because at high densities the second solvation shell may make

an additional contribution and $N_{clus}^{(2)}$ still makes a contribution at high densities. When the outer wall of the solvation shell is extended to about 30% of the original width of the solvation shell, the increase of the solvation number can be smoothly connected between the regions of two kinds of compression regime.

III. Effects of Solvation on Energy Transfer and Chemical Reactions in Supercritical Solutions

A. Energy Transfer and Dissipation

Energy transfer in the gas and liquid phases is a fundamental processes controlling the rate of chemical reactions. In the transition-state theory, the thermal equilibrium is assumed all through the reaction process and in the RRKM theory the complete energy randomization within a microcanonical ensemble is the basic prerequisite. When the collisional energy transfer takes place much faster than the barrier crossing, the reacting system could be maintained in thermal equilibrium with the heat bath. In the same way when the collision-induced intramolecular energy transfer is very efficient, the complete randomization of energy within a reacting molecule could be achieved. In the low-pressure limit, however, the actual reacting system may proceed under nonequilibrium conditions. Then, the collisional energy transfer rate as a function of density/pressure is quite important in determining the fundamental environment for reactions.

Usually in the liquid phase the energy transfer or dissipation is expected to occur much faster than any reactive processes and hence the complete equilibrium or the establishment of the Boltzmann distribution is assumed as a basis of reaction rate theories. On the other hand, in the gas phase, the energy transfer is a bimolecular event and hence the collision number with bath gas molecules is the fundamental quantity in determining the rate of energy transfer. To extrapolate the gas phase theory to liquid phase, one has to define the collision number in the liquid phase. However, in the dense gas or the liquid phase, it is difficult to define the separate bimolecular collisions, since the average distance between the energized molecule and the solvent molecules is in the order of the collision diameter defined in the gas phase. Furthermore, the bimolecular collision may not be an independent event but a significant number of termolecular collisions could occur in the dense environment. In this sense the observation of the energy transfer rate with varying density is quite interesting from both the experimental and theoretical viewpoints.

1. The Independent Binary Collision Model

A simple method for estimating the collision number in the liquid phase is proposed by Helzfeld and Litovitz as "Independent Binery Collision (IBC) model".[78,79] They have assumed that the rate of vibrational energy transfer causing the $i-j$ transition in the liquid phase, k_{ij}, can be expressed as

$$k_{ij}(\rho,T) = P_{ij}(T)Z_{liq}(\rho,T) \tag{20}$$

where P_{ij} is the energy transfer probability per collision and assumed to be independent of the density of the liquid. Z_{liq} depicts the collision number in the liquid phase, and usually estimated from the gas-phase collision rate Z_{gas} and the values of the radial distribution functions, $g_{lig}(r^*)$ and $g_{gas}(r^*)$, at a critical distance where the energy transfer mainly occurs, i.e.,

$$Z_{liq} = Z_{gas}\frac{\rho_{liq}g_{lig}(r^*)}{\rho_{gas}g_{gas}(r^*)} \tag{21}$$

where ρ_{gas} and ρ_{liq} denote the bulk density of gas and liquid phases, respectively. This simple treatment offers reasonable estimation of the energy transfer in the liquid phase in many cases. For example, Simpson and co-workers[80,81] investigated the energy transfer between N_2 and NO in both gaseous and liquid xenon at the same temperature and found that the rate constant for the nonresonant ($\Delta E > 150$ cm^{-1}) V−V energy transfer was the same in the both phases. Harris and co-workers studied the vibrational relaxation of hot I_2 molecule in liquid Xe of various densities[82,83] and found that the IBC model is correct even for the molecular system with large amplitude motions (170−210 cm^{-1}). However, for near-resonant V−V transfer where ΔE is small and $\Delta E/h$ becomes closer to collision frequency, IBC model seems to be inadequate in predicting the rate constant in liquid phase.[84]

For the energy dissipation in polyatomic molecules, Troe and co-workers have reported a series of experiments using highly vibrationally excited S_0 molecules. Schwarzer et al.[85] studied the deactivation of highly excited ground-state azulene in supercritical fluids of varying densities. Azulene molecules were excited to S_1 state with a subpicosecond laser pulse at 620 nm and allowed to make rapid internal conversion to highly vibrationally excited S_0 state. The deactivation was followed by using the probe pulse at 580−600 nm which excited the deactivating S_0 azulene molecules to S_2 state. They found that the decay of the average energy, $\langle E\rangle$, of the excited azulene molecule was expressed by the exponential form

$$\langle E(t)\rangle = \langle E_0\rangle \exp(-t/\tau_c) \tag{22}$$

They first measured the phenomenological cooling time, τ_c, for various solvent gases at low pressure. The cooling rate, $1/\tau_c$, is considered to be proportional to the collision number Z at low pressure, and the proportional constant depends on the energy transferred per collision with a selected bath gas molecule, $\langle\Delta E\rangle$, as

$$\frac{1}{\tau_c} = \frac{\langle\Delta E\rangle}{\langle E\rangle}Z \tag{23}$$

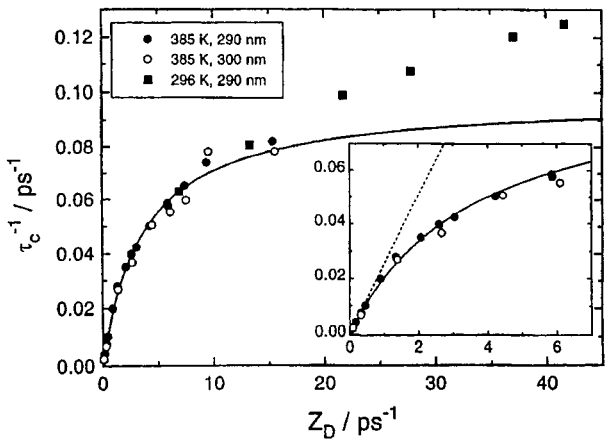

Figure 14. Collision frequency dependence of τ_c^{-1} for energized azulene molecule in supercritical C_2H_6, together with the prediction by the Langmuir-type adsorption model. The collision frequency Z_D is calculated by using the modified IBC model. (Reprinted with permission from ref 85. Copyright 1996 American Institute of Physics.)

They examined whether this relation could hold at high density, using the collision frequency, Z, derived by the independent binary collision (IBC) model with the use of eq 21 but using solvent self-diffusion constant D instead of the radial distribution function $\rho g(r)$. Then they found $\langle \Delta E \rangle$ in both dilute gas and supercritical fluid to be quite similar for He up to very high densities. However, for other gases such as N_2, Xe, CO_2, and C_2H_6, $\langle \Delta E \rangle$ gradually decreased above the density of 1 mol/L. As Figure 14 shows, the dependence of τ_c^{-1} on the collision frequency predicted by the *modified* IBC model is not linear as depicted by the broken line but with a significant curvature. This fact indicates that the evaluation of collision number by the modified IBC model is no longer valid at high densities for these gases. A similar trend was observed for the collisional deactivation of cyclooctatetraene in compressed supercritical fluids.[86]

To interpret the leveling-off behavior of τ_c^{-1}, Schwarzer et al. proposed three possibilities. The first possibility is the ineffective heat transfer from the first solvation shell to solvent molecules outside. However, the macroscopic thermal conductivity is even larger than the observed heat transfer rate. The second interpretation is the incomplete IVR in the azulene molecule, which could retard the energy flow to the environment. This interpretation, however, cannot explain the large difference between He and Xe in the energy transfer efficiency. The final possibility is the clustering. Clustering of solvent could suppress the energy dissipation through the collisions with outer solvent molecules because of the indirect contact of colliding molecules with the azulene molecule. In other words, clustering solvent molecules act as a shielding against the efficient energy transfer. On the basis of the final possibility, Schwarzer et al. calculated the clustering number using the Langmuir-type model[55] and found that the observed trend could be reproduced up to the fairly large densities for various gases. The solid line in Figure 14 depicts the trend predicted by the cluster model. This model, however, could not reproduce the further increase of the energy transfer rate in much higher density region.

Recently, Schwarzer et al.[75] compared the energy transfer rate of hot azulene with the spectral shift in the absorption spectrum of the same molecule under the same condition. They found that the density dependence of these two quantities perfectly coincided with each other. To explain the density dependence, they used the *standard* IBC model assuming the constant energy transfer probability per collision. They evaluated the radial distribution function of solvent molecules around the solute molecule using Monte Carlo simulations with Lennard-Jones potentials for solvent−solute and solvent−solvent interactions. The density dependence of the collision number was found to be in excellent agreement with the trend observed in the density dependence of the energy transfer rate. They also demonstrated that with the use of the same radial distribution function, the observed density dependence of the spectral shift was well reproduced. These results strongly suggest that both the energy transfer and the spectral shift reflect the environment of direct vicinity of the azulene molecule, i.e., the first solvation shell.

2. A Fluctuation Model

Fayer and co-workers have examined the energy relaxation process in dense gases using a carbonyl compound, $W(CO)_6$, whose CO stretching vibration was excited to $v = 1$. Urdahl et al.[68,69] studied the relaxation process of vibrationally excited $W(CO)_6$ by a pump−probe technique using picosecond IR pulses.[87] Their results are shown in Figure 15. In supercritical CO_2 at 33 °C which is just above the critical temperature, the lifetime T_1 of the vibrationally excited $W(CO)_6$ first decreases smoothly from 900 ps at 0.09 g/cm^3 to 700 ps at 0.22 g/cm^3 and then stays at the almost constant value of 670 ps between 0.3 and 0.65 g/cm^3 and again starts decreasing above 0.65 g/cm^3. On the other hand, at 50 °C which is sufficiently above the critical temperature, the above tendency of forming the plateau becomes weak. They also measured the bathochromic shift of CO stretching vibrational frequency with increasing density in supercritical CO_2 at 33 and 50 °C, and found that its density dependence was in close parallel to the lifetime of vibrationally excited $W(CO)_6$ at both temperatures as shown in Figure 15.

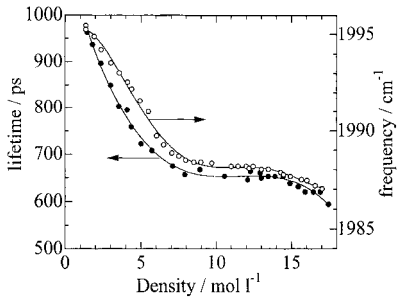

Figure 15. Lifetime of vibrationally excited $W(CO)_6$ and the bathochromic shift of CO stretching vibrational frequency with increasing density in supercritical CO_2 at 33 °C. The plots are based on the data by Urdahl et al. (ref 69).

To explain the observed trend, Urdahl et al. proposed a theory based on the force correlation function formalism[88,89] combined with the thermodynamic properties of supercritical fluids.[90] With the Hamiltonian for the harmonic oscillator of mass m and natural frequency of ω under the influence of fluctuating force $F(t)$ by solvent molecules

$$H = \frac{p^2}{2m} + \frac{1}{2} m\omega^2 x^2 + F(t)x \tag{24}$$

where x and p denote the displacement and the momentum of the oscillator, the vibrational relaxation rate can be expressed as a Fourier transform of a classical force autocorrelation function as

$$T_1^{-1} = \frac{1}{m k_B T} \int_0^\infty \mathrm{d}t \langle F(t)F(0)\rangle_{\mathrm{cl}} \cos(\omega t) \tag{25}$$

They evaluated the force autocorrelation function using bulk properties of fluids such as thermal compressibility κ_T, the thermal diffusivity D_T, and the correlation length ξ. After elaborate manipulation of the equation using relations among these quantities and a number of approximations, they finally derived the equation at the limit of $k\xi \gg 1$,

$$T_1^{-1} \propto T \frac{\rho_1 \kappa_T/\kappa_T^0}{\xi^2} \hat{C}_{21}(k=0) \int_0^\infty \mathrm{d}t \cos(\omega t) \int \mathrm{d}\boldsymbol{k} \times \exp(-D_T \xi k^3 t) \tag{26}$$

where ρ_1 denotes the solvent density and $\hat{C}_{21}(\boldsymbol{k})$ is the Fourier transform of the two-particle direct correlation function $c_{21}(\boldsymbol{r})$ between solute and solvent

$$\hat{C}_{21}(\boldsymbol{k}) = \int_0^\infty \mathrm{e}^{-i\boldsymbol{k}\cdot\boldsymbol{r}} c_{21}(\boldsymbol{r}) \, \mathrm{d}\boldsymbol{r} \tag{27}$$

$\hat{C}_{21}(\boldsymbol{k})$ could be approximated by $\hat{C}_{21}(0)$, since $\hat{C}_{21}(\boldsymbol{k})$ at large $\boldsymbol{k}$ makes small contribution near the critical point.

On the basis of eq 26, they examined the variation of T_1^{-1} near the critical point and found that the three quantities, $[(\rho_1\kappa_T)/\kappa_T^0)/\xi^2$, $D_T\xi$, and $\hat{C}_{21}(0)$, in the equation were all insensitive to the density. The calculated density dependence of T_1 well reproduced the observation. Since they only used the thermodynamic properties of fluids, they claimed that the microscopic concept of cluster was not necessary to explain the observed insensitivity of the vibrational relaxation rate to the density near the critical point.

Urdahl et al. further demonstrated that the IR spectral shift $\Delta\nu$ could also be expressed in terms of the above quantities near the critical point as

$$(\Delta\nu)^2 \propto T^2 \frac{\rho_1 \kappa_T/\kappa_T^0}{\xi^2} \hat{C}_{21}(0)^2 \tag{28}$$

and again pointed out that the invariance of the frequency shift near the critical point was explainable within the framework of the fluctuation formalism. Mayer et al.[91] measured the temperature dependence of the lifetime of vibrationally excited $W(CO)_6$ near the critical densities. The lifetime increases between 300 and 370 K and then decreases at higher temperatures. According to their theory based on the classical force autocorrelation function, the lifetime should decrease monotonically with increasing temperature. Although they suggested the inclusion of the quantum correction into the classical theory to improve the agreement, they have not yet come up with a reasonable way of quantum corrections.

It should be pointed out here that the above treatment based on the autocorrelation function contains so many approximations and assumptions. In particular, the replacement of the integral of $\hat{C}_{21}(\boldsymbol{k})$ with constant $\times$ $\hat{C}_{21}(0)$ could lose the information of molecular interaction with solvent molecules of immediate vicinity. The density and temperature dependence of the terms appearing in the above equations should be evaluated carefully in the approximation procedures.

3. IVR and Energy Dissipation

The energy transfer process from a highly excited chromophore molecule to the environment could be divided into two successive processes. The first process is the intramolecular energy redistribution (IVR) within the chromophore molecule and the second one may be the energy dissipation from this fully energy randomized molecule to the bath gas or solvent molecules. The solvent molecules in the first solvation shell may be involved in the first process. Ordinarily, this first process takes place quite rapidly and the majority of the experiments report the time history of the second process.

In the vibrational relaxation of azulene given in section II.A.1, the vibrational energy in highly vibrationally excited azulene is probably well randomized among various vibrational modes throughout the process of energy dissipation to solvent fluid molecules. The vibrational mode coupling in the $S_1 \rightarrow S_0$ internal conversion and also the presence of many vibrational modes in azulene as well as the large excess energy help the excess energy to be distributed randomly before the energy dissipation starts. On the other hand, in the experiments using $W(CO)_6$ the vibrational population in a specific vibrational mode of the chromophore molecule was detected. It is therefore not certain whether the vibrational energy is transferred to solvent molecules (dissipation) or into other vibrational modes of $W(CO)_6$ (IVR). In actual events, it may be difficult to discriminate the energy dissipation to solvent from the IVR process. These processes could occur simultaneously because the solute molecule and closely located solvent molecules form a kind of complex and the intermolecular vibrations within the complex could participate in the IVR process. Such phenomena are observed in rigid van der Waals complexes formed in a supersonic jet.[92]

From the above viewpoint, the density dependence of the rates for both IVR and energy dissipation is quite interesting, particularly, in the supercritical region. At low densities, clusters are well distinguished from the bulk area. The clusters in such situation, may provide a chance to discriminate the rapid IVR within the cluster, the chromophore plus

several solvent molecules, from the slow energy dissipation to distant solvent molecules through collisions. The observation of both the energy loss from the chromophore and the energy gain in solvent molecules is critical for such discrimination. Recently, in the liquid phase, the energy dissipation was found to occur much faster than expected. Using thermal grating technique, Terazima[93] observed very rapid (~3 ps) heating of solvent H_2O after exciting the chromophore ion Ni^{2+}. The mode dependence of the energy dissipation rate was also suggested in the vibrational energy transfer from vibrationally excited S_1 *trans*-stilbene to solvent molecules.[94] Further studies are necessary to elucidate the energy dissipation process in the condensed phase.

B. Rotational Relaxation

The study of rotational relaxation in liquids has a long history. The basic idea was provided by the Stokes−Einstein−Debye (SED) equation[95−97] which relates the rotational reorientational time τ_r with the hydrodynamic viscosity η of the solvent and the volume of a rotating spherical molecule V as

$$\tau_r = \frac{\eta V}{k_B T} \tag{29}$$

For any general molecules, the equation can be modified as

$$\tau_r = \frac{\eta V}{k_B T} f_{stick} C + \tau_0 \tag{30}$$

where τ_0 is the rotational reorientational time at zero viscosity and qualitatively related to the free-rotor correlation time. The shape factor f_{stick} is a well-specified dimensionless hydrodynamic frictional coefficient for stick boundary condition and only depends on the shape of a solute molecule. For example, f_{stick} of a prolate spheroidal with a ratio A of its longitudinal to axial dimensions can be calculated as[98]

$$f_{stick} = \frac{2(A^2+1)(A^2-1)^{1.5}}{3A\{(2A^2-1)\ln[A+(A^2-1)^{0.5}] - A(A^2-1)^{0.5}\}} \tag{31}$$

The boundary condition parameter C expresses the effect of solute−solvent boundary and is strongly dependent on the shape of the solute, the solute−solvent interaction, and the solvent density. In the majority of cases, the boundary condition is taken to be "stick". That is, the solvent molecules in the first solvation shell coherently rotate with the solute molecule. When the solute molecule is spherical, both f and C are set equal to unity and the equation is reduced to the original SED equation. On the other hand, for the "slip" boundary condition, where the solvent molecules do not rotate, C becomes zero for a spherical solute molecule; the spherical solute molecule rotates freely and is independent of surrounding solvent molecules. When the molecular shape is not spherical but spheroidal, friction is operative between the solute and solvent molecules even in the slip case, because the rotation of a nonspherical molecule inevitably causes the displacement of solvent molecules. The selection between the stick and slip conditions largely depends on the relative molecular size of the solute and the solvent molecules. When the solute molecule is much larger than the solvent molecule, the stick condition holds in most cases, whereas the rotation of a relatively small solute molecule is better expressed by the slip model. This is due to the interstitial space formed by solvent molecules where the small solute molecule can rotate freely. In this sense, the microscopic molecularity now enters into the macroscopic hydrodynamic formalism.

Following the original proposal of slip conditions by Hu and Zwanzig,[99] several research groups have developed methods for evaluating C in a variety of conditions. The most commonly used is the Dote−Kivelson−Schwartz (DKS) equation based on their quasihydrodynamic free volume model.[100] In the DKS equation, C is given by

$$C = [1 + \gamma/\phi]^{-1} \tag{32}$$

with

$$\gamma = \left(\frac{\Delta V}{V_P}\right)[4(V_P/V_S)^{2/3} + 1] \tag{33}$$

where V_P and V_S denote the volume of the solute and solvent molecules, respectively. ϕ is a factor expressing the ratio of the effective rotational volume to V_P. When the solute−solvent interaction is small, ϕ could be taken to be f_{stick} to a first approximation. ΔV is the smallest volume of free space per solvent molecule and can be represented as

$$\Delta V = B\kappa_T \eta k_B T \tag{34}$$

using hydrodynamic quantities such as κ_T and η, and the constant parameter B which is independent of temperature.

As being apparent from the above explanation, the microscopic features due to the molecular interaction between the solute and solvent molecules are all confined into the constant C. Despite its simplicity, the above formalism has successfully explained, at least qualitatively, a variety of solute−solvent systems in the liquid phase.[100−102] The ordinary way of comparison is to plot the measured rotational reorientation time against (η/T). According to the eq 30, the slope and the intercept of the linear plot correspond to VfC/k_B and τ_0, respectively. In some cases, however, the linear plot is not appropriate to express the relation between τ_r and η/T, which suggests modifications to the above treatment are needed.

Experimentally, various methods have been used to obtain the rotational reorientational time. The most direct technique is to measure the anisotropy decay of fluorescence using picosecond laser system.[103] The steady-state anisotropy measurement in fluorescence, combined with the fluorescence lifetime measurement, has also been used.[102] Further-

more, NMR spin−lattice relaxation times [104,105] and the evaluation of rotational diffusivity by simulating ESR spectra[106] provide the correlation time for a second-rank Legendre polynomial component $P_2(\cos\theta)$. Although, for symmetric top molecules, τ_r can be different for rotations parallel and perpendicular to the top axis, one usually obtains a single weighted average correlation time or the longer value of the two correlation times.

Supercritical fluids, as discussed in the previous section, can provide a variety of environmental conditions for the energy transfer experiments, from collision-controlled gaslike conditions to diffusion-controlled liquidlike conditions. In addition, they also provide various degrees of density fluctuation which might affect the relaxation time. Such consideration urged scientists to measure the rotational reorientation time in supercritical fluids. Anderton and Kauffman[107] measured the rotational correlation time of *trans,trans*-1,4-diphenylbutadiene (DPB) and *trans*-4-(hydroxymethyl)stilbene (HMS) in supercritical CO_2 at 35 °C with a stationary anisotropy technique. They found that in both cases the rotational correlation time increases with increasing fluid density between 0.3 and 0.8 g/cm^3. To relate these correlation time with the density augmentation or local density around a rotating solute molecule, they have propose a modified DKS model which explicitly includes the local density of fluid as

$$\tau_r = \frac{\eta(\rho_{12}^l)V}{k_B T} f_{\text{stick}} C(\rho_{12}^l) + \tau_0 \qquad (35)$$

where the local density ρ_{12}^l is defined as

$$\rho_{12}^l(R) = \rho(1 + F(g_{12}(r))) \qquad (36)$$

The local density parameter, $F(g_{12}(r))$, is an integral equation in the radial distribution function $g_{12}(r)$ of solvent molecules and expresses the excess solvent density in the region of a solute molecule. R represents the radius of the first solvation shell. The local solvent viscosity $\eta(\rho_{12}^l)$ is calculated from the density expansion of viscosity whereas $C(\rho_{12}^l)$ is estimated according to the DKS method except the evaluation of ΔV using the relation:

$$\Delta V = \frac{M}{\rho_{12}^l} - V_{\text{s,vdW}} \qquad (37)$$

where M denotes the solvent molar mass and $V_{\text{s,vdW}}$ means the van der Waals volume of the solvent molecule. The analysis using the above equations showed that, in the case of DPB, $F(g_{12}(r))$ is nearly zero with a possible small positive value at low densities whereas HMS gave the value of 0.4 for $F(g_{12}(r))$ in all the density region. This result suggests that the rotational correlation time is influenced by the solute-induced clustering with varying extent depending on the solute−solvent interaction.

Heitz and Bright[108] measured the rotational reorientational time of *N,N′*-bis-(2,5-*tert*-butylphenyl)-3,4,9,10-perylenecarboxodiimide (BTBP) in supercritical CO_2, CF_3H, and C_2H_6 at the reduced temperature $T^* = 1.01$ with a phase modulation technique. In all three supercritical fluids, the rotational reorientational time was unexpectedly long and decreases with increasing fluid density $\rho^*(=\rho/\rho_c)$ between 1.4 and 1.9 as shown in Figure 16. At the highest density, the reorientation time approaches the value of hydrodynamic prediction. Applying the above-mentioned Anderton−Kauffman method to the observed data, they concluded the local density to be 3 times larger than the bulk density ($\rho^* = 0.9$). However, such a high augmentation ratio indicates that the local density at $\rho^* = 0.9$ exceeds the liquid density, which is quite puzzling.

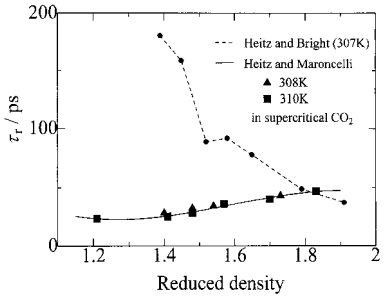

Figure 16. Rotational reorientational time of BTBP as a function of fluid density $\rho^*(=\rho/\rho_c)$ between 1.2 and 1.9. The experimental results from Bright's and Maroncelli's groups are compared. The plots are based on the data by Heitz and Bright (ref 108) and by Heitz and Maroncelli (ref 103).

Simulating the bandwidth of ESR spectra with the parameters for rotational diffusivity and Heisenberg spin exchange rate, de Grazia et al.[106] estimated the rotational correlation time of copper 2,2,3-trimethyl-6,6,7,7,8,8,8-heptafluoro-3,5-octanedionate (Cufod) in supercritical CO_2 at 35 °C. At low fluid densities ($\rho^* = 0.7-0.8$), they also reported an extremely long correlation time, which decreases with increasing density and approaches the value predicted by the SED model at the highest density ($\rho^* = 1.8$). The Anderton−Kauffman analysis again suggests that the local density at $\rho^* = 0.7$ is by a factor of 4 larger than the bulk density. The derived local density is even larger than the highest bulk density used in their experiments.

Recently, Heitz and Maroncelli[103] determined the rotational correlation times of 9,10-bis(phenylethynyl)anthracene (PEA) and BTBP both in liquid hydrocarbons and in supercritical CO_2 at 35 °C with picosecond time-domain measurements of fluorescence anisotropy. They found that the correlation time was as short as 25 ps for BTBP at $\rho^* = 1.4$ and increased with increasing density, contrary to the previous work by Heitz and Bright[108] who reported the value of 180 ps at the same density. Comparing with the predictions by the hydrodynamic formalism discussed above, Heitz and Maroncelli concluded that the behavior of BTBP is quite normal, whereas that of PEA deviates significantly from the prediction near the critical point. The observed trend for PEA suggests that local density augmentation leads to increased rotational friction on the solute rotation and an effective density must be 50−100% greater than the bulk density in the region of $\rho^* = 0.8-1.0$. The difference in the density dependence in the rotational

correlation time between BTBP and PEA could be attributed to the different density region used for each experiment; the PEA experiment was performed near the critical density, whereas the BTBP experiment was conducted at higher densities due to its low solubility. At the density region close to or lower than the critical density, the local density is certainly higher than the bulk density by about 50−100% depending on the solute−solvent interaction. Heitz and Maroncelli also measured the spectral shifts of PEA and BPBT and estimated the density augmentation around these solute molecules in supercritical CO_2. The augmentation estimated from the spectral shifts were completely in parallel with that estimated from the rotational correlation times. They suggested that the discrepancy between the two observations, theirs and those by Heitz and Bright, could be due to the wavelength selected for fluorescence detection; the wavelength chosen by Heitz and Bright may be significantly affected by the solvent Raman band.

Although there are some disagreement in the observed density dependence of the rotational correlation time among the researchers, all agree that the solvent density augmentation occurs in supercritical fluids and significantly affects the solute rotation. As pointed out by Heitz and Maroncelli, the parallelism between the spectral shift and the rotational correlation time is quite interesting since these two phenomena are different in their nature, static and dynamic, and hence may have different length scale in their effective solute−solvent interaction. As stated in the preceding section, the density dependence of vibrational energy dissipation was also in parallel to that of the spectral shift.

C. Diffusion Controlled Reactions

1. Basic Concept of Diffusion-Controlled Reactions

The diffusion coefficient is also a density dependent hydrodynamic quantity. It decreases monotonically with increasing density or increasing collision number. The diffusion coefficient is defined by the Fick's law, which states that the number of molecules moving in the x direction through a cross sectional area of S per unit time is proportional to the concentration gradient in that direction, that is,

$$\frac{\mathrm{d}n}{\mathrm{d}t} = -DS\frac{\mathrm{d}c}{\mathrm{d}x} \tag{38}$$

where n and c represent the number and the concentration of molecules (= the number of molecules per unit volume), respectively, and D is the diffusion coefficient. The negative sign indicates that the diffusion occurs in the direction of decreasing concentration. In the low-pressure limit, a simple gas-kinetic calculation for hard-sphere gas gives the formula for the self-diffusion coefficient for a molecule of mass m as

$$D = \frac{1}{2}\bar{v}\lambda = \frac{1}{\pi\sigma^2 c}\sqrt{\frac{k_\mathrm{B}T}{\pi m}} \tag{39}$$

where $\bar{v}$, λ, and σ represent the mean velocity, the mean free path, and the collision diameter of the molecule, respectively. This equation indicates that the diffusion coefficient is inversely proportional to the concentration c or the density of the gas.

On the other hand, the diffusion coefficient for a spherical molecule of radius r in a medium with viscosity η can be expressed by the Stokes−Einstein equation as

$$D = \frac{k_\mathrm{B}T}{6\pi\eta r} \tag{40}$$

This equation is known to be appropriate for liquids or high-pressure gases. Thus, the diffusion coefficient is inversely proportional to the collision number at low density, whereas at high density the collision number is replaced by viscosity. In the density region of supercritical fluids, the transition between these two expressions must occur in parallel with the increasing ambiguity in the definition of collision number. Troe and co-workers therefore proposed to use the inverse diffusion coefficient as a measure of effective collision number for compressed gases.[8,109−111]

In low-pressure gas, the maximum rate of a bimolecular reaction without activation energy could be the collision frequency and such a reaction is called "gas kinetic". In the liquid phase, however, the diffusion process controls the encounter of two reactant molecules and hence the bimolecular reactions occurring in every encounter in solution are often called "diffusion-controlled" reactions. A typical rate constant for the diffusion-controlled reactions is around 10^{11} dm^3 mol^{-1} s^{-1}. The rate of a diffusion-controlled reaction can be derived by considering a model where a reactant molecule B approaches to another reactant molecule A with the diffusion coefficient D. The reaction is assumed to occur with unit probability when B reaches the spherical boundary of radius R around the reactant molecule A. Then, the rate of the bimolecular reaction is equal to the flux of B toward the spherical sink around A, and the rate constant k_D can be evaluated by using the method of Smoluchowski as

$$k_D = 4\pi(D_\mathrm{A} + D_\mathrm{B})R \tag{41}$$

where D is replaced by the mutual diffusion coefficient ($D_\mathrm{A} + D_\mathrm{B}$). In some cases, this equation is expressed as a function of viscosity in place of the diffusion coefficient. To replace the diffusion coefficient with viscosity, the Stokes−Einstein law (eq 40) could be adopted. Using this equation one can rewrite the mutual diffusion coefficient as

$$D_\mathrm{A} + D_\mathrm{B} = \frac{k_\mathrm{B}T}{6\pi\eta}\left(\frac{1}{r_\mathrm{A}} + \frac{1}{r_\mathrm{B}}\right) \tag{42}$$

where r_A and r_B denote the radii of the reactants A and B, respectively, and R equals $r_\mathrm{A} + r_\mathrm{B}$. Furthermore, if the molecular radii are equal, eq 41 can be reduced to a simple form as

$$k_\mathrm{D} = \frac{8k_\mathrm{B}T}{3\eta} \tag{43}$$

In supercritical fluids, the rate of a barrierless bimolecular reaction could be estimated by the above equation at the high density limit. As the density decreases, the approximation as a diffusion-controlled reaction becomes poorer and the rate constant gradually approaches to gas kinetic in the low-pressure limit. The transition, however, cannot be smooth and simple, since the clustering near the critical point may affect the diffusion process and the encounter radius. To investigate these problems, the rates of diffusion-controlled reactions have been measured by several research groups. The three typical diffusion-controlled reactions investigated in supercritical fluids are pyrene excimer formation, Heisenberg spin-exchange reaction between nitroxyl radicals, and triplet−triplet annihilation of triplet benzophenone. Among them, pyrene excimer formation is not truly a bimolecular event since, at low pressures, the excimer needs to be stabilized by a third body just like atom−atom recombination reactions. However, because of its large degrees of freedom, the pyrene excimer is easily stabilized even at low pressures. Therefore, the pyrene excimer formation is effectively considered as a diffusion-controlled bimolecular reaction. The quenching of an electronically excited molecule in S_1 or T_1 state by efficient quenchers could also serve as an example of diffusion-controlled processes, when the lifetime of the excited state is sufficiently long as compared with the diffusive encounter.[112]

2. Pyrene Excimer Formation

Brennecke et al.[113] and Zagrobelny et al.[114,115] studied the excimer formation of pyrene in supercritical CO_2. When an electronically excited pyrene molecule encounters another pyrene molecule within its lifetime, the excimer consisting of two pyrene molecules are formed and the emission from the excimer can be observed around 460 nm. Both research groups found that the excimer emission was greatly enhanced in supercritical CO_2 than in ordinary liquid hydrocarbon solvents. The emission spectra characteristic to the excimer was detectable even at the pyrene concentration of 10^{-5} M in supercritical CO_2, whereas 10^{-3} M was necessary in liquid hydrocarbon solutions. The excimer emission became weaker with increasing fluid density. Zagrobelny et al.[114] determined the forward and backward rate constants by time-resolved fluorescence spectroscopy and found the rate constants for both directions to be 2 orders of magnitude larger than those in liquid solutions. Their observation indicates the equilibrium constant for the excimer formation is not affected by changing the medium from liquid to supercritical fluid.

They also found that the simple Stokes−Einstein−Smoluchowski equation (eq 43) was able to predict both the absolute value and the density dependence of the observed forward rate constant. Since this equation only includes the effect of bulk hydrodynamic viscosity of the solvent, the observed large forward rate constant is merely the consequence of the 2 orders of magnitude smaller viscosity of supercritical CO_2 as compared with that of liquid hydrocarbons. That is, the solvent clustering around the pyrene molecule gives no effect on the excimer formation rate constant in supercritical CO_2.

Then, what is the reason for the enhanced excimer emission? Zagrobelny et al.[114] examined the rate of excimer quenching in supercritical CO_2, which was an order of magnitude slower than that in liquids. They suggested that the clustering by CO_2 molecules around the pyrene excimer acts as a shield and protects the excimer from being quenched by contaminating O_2 or other quencher molecules. If so, the quantum yield of excimer fluorescence is larger in supercritical CO_2 than in liquids; therefore, the fluorescence becomes detectable even for the small equilibrium concentration of the pyrene excimer. Zagrobelny et al.[115] later observed the same behavior in supercritical C_2H_6 as in CO_2. In supercritical CF_3H, however, the excimer formation rate was smaller than the rate predicted from the Stokes−Smoluchowski equation probably because the strong clustering of CF_3H retards the dimer formation when the excited pyrene encounters a solvated ground state pyrene molecule. It should be noted, however, that the fluorescence lifetime of the pyrene excimer is extremely sensitive to the O_2 contamination in fluid or liquid solvents and such contamination could give a significant effect on the above observations.

3. Heisenberg Spin Exchange

Heisenberg spin-exchange reactions between free radicals are typical collision-controlled rapid reactions in which the radicals with antiparallel spin exchange their spin states. These reactions have been studied with an electron spin resonance (ESR) technique. The spectral shape, the line width in particular, is simulated by fitting the two parameters, the spin-exchange rate and the spin−rotation interactions; the latter parameter alone is obtained at extremely diluted conditions.

The rate constant for the spin-exchange, k_e, can be expressed as

$$k_e = k_D p_R = k_D \frac{1}{2} \frac{J^2 \tau_C^{\,2}}{1 + J^2 \tau_C^{\,2}} \qquad (44)$$

where p_R is the reaction probability. J represents the exchange integral which only depends on the molecular properties of the radical. The collision time τ_C means the time interval between collisions and corresponds to the interaction time for the radical pair. In liquid solutions, the combined use of the above equation with the Stokes−Einstein−Smoluchowski (SES) equation of diffusion-controlled rate constants generally gives a reasonable estimate of k_e.

Randolph and Carlier measured the Heisenberg spin-exchange rate of *tert*-butyl nitroxide radical in supercritical ethane.[116] They found that at high densities, the observed exchange rate was in good agreement with the prediction from the SES equation; however, as the density decreases toward the critical density, the observed value became larger than the predicted value as shown in Figure 17.

There are two possible explanations to the above-mentioned deviation; one is the effect of clustering and the other is the limited applicability of the SES

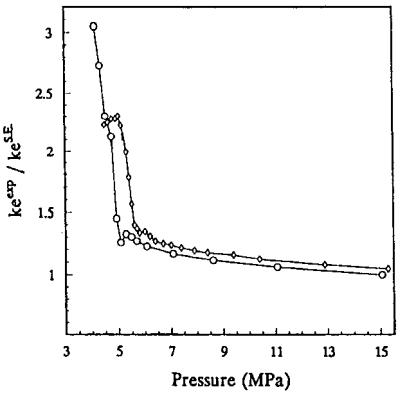

Figure 17. Heisenberg spin-exchange rate of *tert*-butyl nitroxide radical in supercritical ethane at 308 K (circle) and 313 K (diamond). The ordinate is the ratio of the observed bimolecular rate constant to that predicted from the Stokes−Einstein equation as a function of fluid pressure. (Reprinted from ref 116. Copyright 1992 American Chemical Society.)

equation to the lower density gases. The cage formed by the clustering solvent molecules around the colliding radicals may lengthen the interaction time available for the spin exchange, resulting in the enhancement of the exchange rate. However, if such an effect is responsible for the enhancement, the rate should be much enhanced in the high-density region where the solvent cage is expected to be thick and dense. Thus, the cage effect cannot be the reason for the enhancement observed in the critical region. Another explanation is the inadequacy of the SES equation. Although Randolph and Carlier estimated the exchange rate from the SES equation using the viscosity of supercritical ethane,[117] the SES equation itself may not be adequate for reactions in medium-density fluid near the critical point. The transition in the mechanism of rapid bimolecular reactions, i.e., from *diffusion*-controlled to *collision*-controlled, could occur even around the critical density.

Recently, Batchelor[118] measured the Heisenberg spin-exchange rate between nitroxyl radicals (2,2,6,6-tetramethyl-1-piperidinyloxy, TEMPO) in supercritical *n*-hexane and methanol and obtained the results similar to those of Randolph and Carlier. To reproduce the enhancement of the exchange rate at lower densities, he assumed the collision time τ_C to be inversely proportional to the solvent density,

$$\tau_C = (k_D[\text{solvent}])^{-1} \qquad (45)$$

and obtained better agreement at lower densities. This equation simply includes the effect of binary collisions which decrease with decreasing density and thereby increases τ_C, resulting in the increase in reaction probability p_R. The success of such modification again indicate the hydrodynamic regime is inapplicable at low densities.

4. Triplet–Triplet Annihilation

The triplet−triplet annihilation (TTA) process

$$^3B + {}^3B \rightarrow {}^1B^* + {}^1B$$

in normal liquid solvents is known to be a typical diffusion-controlled reaction.[119,120] Roberts et al.[121,122] measured the rate of the TTA process of benzophenone triplet in supercritical CO_2, C_2H_6, and CF_3H with a combination of laser flash excitation of benzophenone and time-resolved transient absorption detection of its triplet. Their data were in good agreement with the diffusion-controlled bimolecular rate constant derived by the SES equation in the wide pressure range of 7.5−30 MPa at various temperatures when the spin statistics factor (= $^5/_9$) for the reaction was taken into account. To estimate the diffusion-controlled rate constant precisely with the SES equation, they measured the viscosity and the diffusion coefficient in the pressure and temperature range used in their kinetic experiments. The estimated rate constants agreed perfectly with the observed ones and no deviation due to the effect of clustering on this diffusion-controlled reaction was observed. They also examined the rate constants for the benzyl radical recombination followed by the laser flash photolysis of dibenzyl ketone in the same supercritical fluids. The obtained rate constants showed again in good qualitative agreement with the rate constants predicted by the SES equation and there was no indication of the effect of clustering.

5. Effect of Clustering on the Diffusion-Controlled Reactions

As pointed out by Troe,[8] the above-mentioned reactions must show the transition from the diffusion-controlled regime to the binary collision-controlled regime with decreasing pressures. Although, in the above example, the low-pressure limit cannot be achieved because of the low solubility of reactant molecules in supercritical fluids, the indication of the onset of transition was clearly observed.

In all three reactions, the simple Stokes−Einstein−Smoluchowski (SES) formalism can well reproduce the rate constants in the high-density supercritical fluids ($\rho \gg \rho_C$). As the density decreases toward the critical density, the rate constant becomes larger than the prediction by the SES equation. The reason for this deviation is not due to the effect of clustering but to the inapplicability of the SES formalism to lower density medium, that is the onset of the transition to the collision-controlled regime. In the case of triplet−triplet annihilation, however, Roberts et al.[121,122] showed that the SES equation can fit the date even down to the critical density when the measured viscosity value is used instead of the estimation using the extrapolation formula. This means that the SES equation may be used in the transition region if the hydrodynamic viscosity is correctly evaluated. However, at the density much lower than ρ_C, one should not use the SES equation for estimating the rate of these reactions, since the Smoluchowski equation becomes inapplicable.

In conclusion, there is no indication of the participation of clusters in the process of diffusion controlled reactions. Although Zaglobelny et al.[114,115] pointed out that the clustering solvent molecules protected the excimer from being quenched by O_2 or other contaminating component, clusters exerted no effect on the diffusion process itself. This is not surprising when

one notices the large difference in the time scale between the cluster lifetime and the diffusion process in supercritical fluids. Diffusion is a rather slow hydrodynamic process as compared with the 1−10 ps lifetime of the clusters estimated from MD simulations.[35,36] The solvent molecules forming a transient cluster repeat the attachment and detachment processes very rapidly and are almost indifferent to the slow movement of solute molecules. In the supercritical state, the kinetic energy between the solute and solvent molecules are about equal to the intermolecular potential energy; therefore, the drag by the clustering solvent molecules has no significant effect on the movement of the solute molecule even though the intermolecular attractive potential has a fairly deep well. Thus, the solvent molecules would not retard the diffusion-controlled reactions, although the solvent molecules around the solute can still exert electronic interaction on the central solute molecule to cause the spectral shift.

The reactions reviewed in the preceding sections were performed in the density region where the density augmentation by clustering is not appreciable and the transition from diffusion control to collision control could not be observed. Although Batchelor[118] took the transition into account to some extent in his analysis of data in low-density region, no detailed observation nor theoretical analysis for the transition region have been conducted yet. For the solute−solvent combination where the strong attractive force or hydrogen bonding is operative, the kinetic energy is not sufficient for the solute molecule to quickly escape from the solvent molecules and the lifetime of the cluster may be prolonged. In such a case, the drag force exerted by solvent molecules may retard the onset of collisional bimolecular processes and consequently the transition to the collision-controlled regime could shift toward lower density than in the case of weak solute−solvent interaction. Further studies are desirable to clarify the behavior of diffusion-controlled reactions in the transition region.

D. Photodissociation and Recombination

In the photodissociation−geminate recombination process as well as in ordinary recombination processes between small radicals, the energy transfer plays a crucial role. In addition, in the photodissociation−geminate recombination process, the presence of the solvent cage is the essential factor in determining the efficiency of the process. Both the cage effect and the energy transfer process dramatically change with varying density of the environment from the gas to liquid states. The studies in supercritical fluid at gas−liquid transition region, therefore, offer rich information on photodissociation and recombination reactions.

1. Atom–Atom Recombination

The atom−atom recombination process at low pressure is a termolecular process, where the collision of a third body gas is necessary to remove the energy from the collision complex formed from recombining atoms. Without the third-body collision, the transient collision complexes with excess energy efficiently

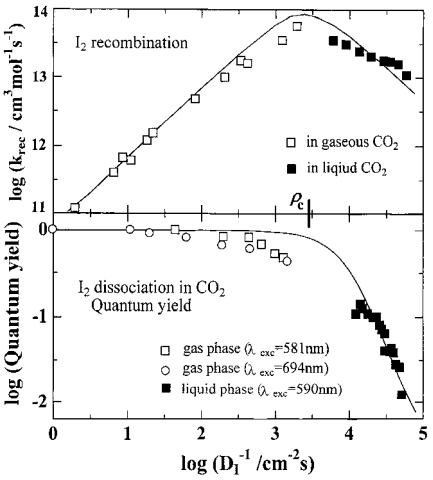

Figure 18. Iodine recombination rate constant k_{rec} and photodissociation quantum yield ϕ in compressed CO_2 as a function of the inverse diffusion coefficient D^{-1}, which is a measure of the effective collision number. The line in the upper figure is based on eq 51. The line in the lower figure is based on the equation similar to eq 50, assuming that the mechanism of the energy relaxation is same for both geminate pair and the bimolecular collision complex. The figure is slightly modified from the Figures 1 and 3 of ref 110. (Reprinted with permission from ref 110. Copyright 1984 American Institute of Physics).

redissociate and the diatomic molecules are never formed except through the negligibly small radiative deactivation process. The important parameter controlling the efficiency of this termolecular recombination is the amount of energy removed per collision of the specific third-body molecule. Usually, polyatomic molecules with large degrees of freedom act as the most efficient energy removers. Although the efficiency is quite low with rare gas atoms, they can still be used as the third body. In any case, the rate of recombination increases with increasing density of the third body gas.

The above simple picture of termolecular collisions cannot be applied in liquids, where the removal of excess energy occurs almost instantaneously by an enormous number of collisions with solvent molecules of immediate vicinity. Instead, the recombination in liquids can be viewed as a diffusion-controlled bimolecular process. Since the rate of diffusion-controlled reaction decreases with increasing density as shown in the preceding section, the *bimolecular* recombination rate passes through the maximum when the medium gradually changes from the low-density gas to the liquid state.

Troe and co-workers investigated the reaction dynamics in the supercritical region to clarify the meaning of collision number in dense media.[8,109,110] In their pioneering studies they measured the atom−atom recombination rate for halogen atoms, especially iodine atoms. The thoroughly studied were the effects of the excitation wavelength, temperatures, and the third body gases and their pressures on the recombination.[110,123] Figure 18 shows a typical plot of the iodine recombination rate constant k_{rec} as a function of the inverse diffusion coefficient D^{-1}, which is a measure of the effective collision number. As expected, the rate increases almost linearly (the

unity slope in the log−log plot) in the low D^{-1} region, whereas in the high D^{-1} region it decreases gradually. The solid line is obtained from the expression

$$\frac{1}{k_{rec}} = \frac{1}{k^{g}_{rec}} + \frac{1}{k_{diff}} \tag{46}$$

k_{deff} is given in the Smoluchowski limit as

$$k_{diff} = 4\pi N_A R D_{A-M} \tag{47}$$

where N_A is the Avogadro number and D_{A-M} denotes the binary diffusion coefficient of A in solvent M. R is the approximate encounter radius which is obtained from the Lennard-Jones diameters σ_A and σ_M as

$$R = \sqrt{2}(\sigma_A + \sigma_M)/2 \tag{48}$$

k^{g}_{rec} is the hypothetical recombination rate constant in the absence of diffusion control, and assumed to be able to extend to higher densities by multiplying the ratio of the effective collision number D^{-1}

$$k^{g}_{rec}([M]) = k^{g}_{rec}([M_0])\frac{D^{-1}([M])}{D^{-1}([M_0])} \tag{49}$$

where $[M_0]$ denotes the low gas density. This rate constant constitutes the left part of the plot in Figure 18 which is linearly dependent on the inverse diffusion coefficient. Although the above equation for k_{rec} appears as a kind of simple interpolation formula, it reproduced the collision number dependence of the recombination rate constant in a wide density range.

When He was used as the third body gas, the diffusion-controlled region cannot be reached even at 6000 bar, whereas the transition was clearly observed for Ar, N_2, CO_2, and ethane. The s-shape dependence of k_{rec} observed in the medium-pressure region of the plot (Figure 18) may be explained by the presence of clusters in this pressure region. Instead of the termolecular reaction, the bimolecular reaction involving the radical−bath gas complex, AM,

$$A + AM \rightarrow A_2 + M$$

may become prominent since the increasing bath gas concentration favors the equilibrium concentration of AM

$$A + M \rightleftharpoons AM.$$

The participation of such complexes in the recombination reaction is clearly demonstrated by the atom-cluster recombination reaction performed in the supersonic jet.[124]

2. Photodissociation and Geminate Recombination

The quantum yield of photodissociation is generally reduced with increasing density of the environment. When a solvent cage is formed around the dissociating chromophore molecule, the fragment produced in the photodissociation may have a good chance to recombine within the cage. This phenomenon is a typical example of the cage effect. The recombination of the fragment pair is called "geminate recombination" which should be distinguished from the ordinary recombination discussed in the preceding section. Figure 18 also shows the observed photodissociation quantum yield of I_2 as a function of bath gas pressure. The unit quantum yield at low density gradually decreases with increasing gaseous pressure up to around the critical density and then rapidly drops to less than 1% in the liquid phase.

The iodine photodissociation consists of several successive molecular processes as revealed by picosecond time-resolved experiments in liquid phase.[125] With the light of 500−700 nm, iodine is excited to its B state, makes an electronic curve crossing to either $a l_g(^3\Pi)$ or the $a'0_b^+(^3\Sigma^-)$ state, and predissociates along these potential curves into two ground-state iodine atoms. These processes as a whole occur very rapidly and are impossible to follow with ns time resolution. The resulting iodine atoms possess a fairly large kinetic energy depending on the excitation wavelength and start to separate. However, the collisions with the solvent molecules of immediate vicinity remove the kinetic energy of the iodine atoms, preventing their escape from the solvent cage. When the pair of iodine atoms loses kinetic energy at a distance r_0 within the solvent cage, they start making "geminate recombination" to either the A/A′ state or the ground X state, followed by the vibrational relaxation in both electronic states. The vibrational relaxation takes 10−100 ps, depending on the complexity of solvent molecules. Of course, some iodine atoms can get out of the solvent shell with probability determined by the initial kinetic energy and the energy removal efficiency of the solvent molecules. These free atoms diffuse through the solvent molecules and each finds a partner atom generated from other iodine molecules. This last process is the ordinary bimolecular recombination reaction discussed in the preceding section.

The time resolution (0.1 μs) of the system which Troe's group used for studying bimolecular recombination was not sufficient for measuring the geminate recombination rate. Instead of the direct measurement, they estimated the rate of geminate recombination using the measured quantum yield of photodissociation and an assumed model of geminate recombination. At $t = 0$, the iodine atoms are located on the sphere of radius r_0 and start diffusing to the inner sink at R or toward outside. When the iodine atoms reach the boundary at $r = R$, they are stabilized to form an iodine molecule with a probability of $k^{g}_{rec}/(4\pi R^2 D N_A)$. Using this model they solved the diffusion equation and obtained the expression for the quantum efficiency as[110]

$$\Phi = 1 - \frac{R}{r_0}\left\{\frac{k^{g}_{rec}}{k^{g}_{rec} + k_{diff}}\right\} \tag{50}$$

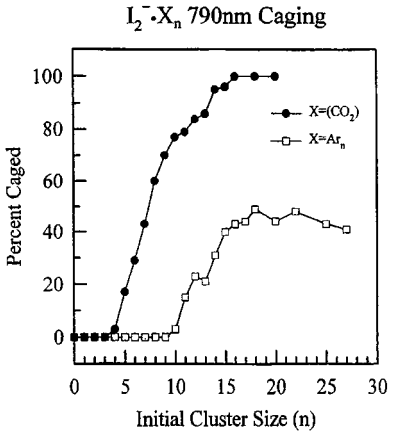

Figure 19. Percentage of geminate recombination of I_2^- in the cage as a function of increasing clustering number in I_2-Ar_n and $I_2-(CO_2)_n$. These data were obtained by using the supersonic jet technique. (Reprinted with permission from ref 126. Copyright 1996 American Institute of Physics.)

The factor in braces corresponds to the probability of energy relaxation within the cage, in competition to diffusion out of the cage. The factor R/r_0 describes the probability of "cage capture" in competition to "cage break-out" during the initial photolysis. As shown in Figure 18, the trend observed in the photodissociation quantum yield in the high-density region was best reproduced with eq 50. It should be noted that if the expression for the nongeminate recombination (eq 46) is rewritten as

$$k_{\mathrm{rec}} \approx k_{\mathrm{diff}}\left\{\frac{k_{\mathrm{rec}}^{\mathrm{g}}}{k_{\mathrm{rec}}^{\mathrm{g}} + k_{\mathrm{diff}}}\right\} \qquad (51)$$

the factor in braces is the same as in eq 50, expressing the competition between the relaxation and diffusion. Therefore, in the above scheme of geminate recombination, the common competition mechanism is assumed for both the geminate complex in the cage and the collision complex formed in the bimolecular atom−atom recombination.

The decrease of the quantum yield in the early stage in low to medium density region is indicated in Figure 18. Troe and co-workers consider this early decrease to be caused by the clustering between the bath gas and molecular iodine before the photolysis,

$$I_2 + M \rightleftharpoons I_2M$$

The attaching bath gas molecule serves as an energy absorber to reduce the kinetic energy of departing iodine atoms, resulting in the reduction of photodissociation quantum yield.

Using solvation clusters formed in a supersonic jet, Lineberger and co-workers[126−129] clearly demonstrated the effect of clustering molecules on the photodissociation quantum yield. As shown in Figure 19, with the increasing clustering number in $I_2^-Ar_n$, the photodissociation quantum yield of I_2^- decreases gradually, and levels off at a certain clustering number where the first solvation shell is filled by the clustering Ar atoms.

The real time measurements of the rapid predissociation and the following geminate recombination process have been conducted by Zewail and co-workers.[130,131] In their comprehensive account published recently, they reported that the vibrational coherence signal lasted for several picosecond even under 2000 bar of He gas.[132,133] Although the dephasing rate increased with the density, the density dependence was rather weak in He and Ne, less than twice between 1 and 2000 bar. From the observed decay of the B state population and the recovery in the A/A′ state population, they evaluated the rates of predissociation from the B state to repulsive surfaces and the rate of geminate recombination to the A/A′ states, respectively. The predissociation rate increased almost linearly with the bath gas density and the difference in the efficiency among the rare gases coincided with the magnitude of their dispersive molecular interactions. The geminate recombination rates including the vibrational relaxation process to the bottom of the A/A′ states were 8×10^{10} s^{-1} and 3×10^{10} s^{-1} for Ar and Ne, respectively, at the pressure of 1200 bar. The probability of geminate recombination was found to be strongly dependent on both the kind of bath gas and its density. For example, the ratio of this probability among He, Ne, and Kr at 1200 bar were found to be 0.02:0.26:1.0, indicating the strong dependence on the molecular interaction. They also reported that the shift of D′ → A′ fluorescence is linearly dependent on the pressure. The simple linearity observed in both the predissociation rate and the spectral shift is reasonable since their experiments were performed at 293 K which is far above the critical temperature of these gases and not favorable for the cluster formation.

3. The Effect of Clustering on Photodissociation and Recombination

As we have learned from the experiments mentioned above, the presence of cluster gives a significant effect on the atom−atom recombination and photodissociation. In contrast to the bimolecular diffusion-controlled reactions, the recombination of atoms or small radicals needs the removal of excess kinetic energy to form a stable molecule and hence the clustering with third-body molecules much enhances the probability of recombination. This behavior is often observed even in a low-pressure region.

Photodissociation and following geminate recombination are strongly affected by the solvent cage. As the density increases, the solvent cage is formed more easily and its effect may become more pronounced. In supercritical fluids, the cage effect appears even in low density region because clusters are easily formed around the solute molecule. Furthermore, in addition to the first solvation shell, the outer shell could also play a role in stopping the flying fragments as suggested by the Lineberger's observation. Thus, the microscopic observation of the size and lifetime of clusters in various supercritical conditions are crucial to understand the photodissociation processes in supercritical fluids. The vibrational energy relaxation of $W(CO)_6$ in various conditions, for example,

could be understood on the same basis as the geminate recombination. We are in need of a unified theory for various energy transfer processes occurring under supercritical conditions.

E. Isomerization

1. Basic Theory of Unimolecular Reactions for a Wide Density Range

The simple but most powerful tool for predicting or analyzing the rate of chemical reactions is the transition-state theory (TST).[134,135] The fundamental assumption in the transition state theory is the complete thermal equilibrium of the reacting system at any point along the reaction coordinate. Although TST almost correctly predicts the absolute rate constant in a variety of reactions, the observed rate constants are usually smaller than the predicted values

$$k = \kappa k_{\mathrm{TST}} \tag{52}$$

where $\kappa(<1)$ denotes a correction factor.

Among the reasons for the deviation from the TST rate, the activation in the reaction valley and the recrossing at the transition state are most significant. The former requires the explicit consideration of the reactant activation process from the bottom of the reactant valley to the top of the potential barrier. This factor becomes crucial in the low-pressure gas-phase reactions where the collisional activation of the reactant is slower than the rate of barrier crossing. The latter factor, recrossing at the transition state, becomes significant for liquid-phase reactions. Although TST assumes the transition state as a "point of no return", solvent molecules in the liquid phase may push the reactant which has already passed the transition state back to the reactant valley, or at least retard the forward motion of the reactant at the transition state region because of their frictional force. The former problem is explicitly treated in the RRKM theory of unimolecular reactions while the latter factor is the primary concern in the Kramers model of one-dimensional barrier crossing.

On the basis of the Lindemann mechanism which explains the falloff curve of the unimolecular reaction rates, the "Rice−Ramsperger−Kassel−Marcus (RRKM)" theory was developed during 1930−1950. The RRKM treatment explicitly takes into account the activation process from the bottom of the reactant valley to the barrier top. Another important feature of the theory is the assumption of complete energy randamization for energized molecules both in the reactant valley and at the transition state.[136] Since the energy randomization occurs quite rapidly for polyatomic molecules with large excess energy, RRKM theory correctly predicts the absolute value and tendency in the temperature and pressure dependence of a variety of unimolecular reactions. In the RRKM scheme, the pressure dependence of unimolecular reaction rates can be expressed as

$$k = \int_{E_0}^{\infty} \frac{k_{\mathrm{a}} F(\epsilon^*)\, \mathrm{d}\epsilon^*}{1 + k_{\mathrm{a}}/(k_{\mathrm{d}}[M])} \tag{53}$$

where $F(\epsilon^*)$ denotes the distribution function of the reactants with the excess energy ϵ^* above the bottom of the reactant potential valley. k_{a} and k_{d} express the rates of the forward reaction and the deactivation, respectively, for the activated reactant molecules with excess energy ϵ^*. Since the rate given by eq 53 approaches the TST rate in the high-pressure limit where $[M] \rightarrow \infty$, the equation can be rewritten as

$$k = \left(\frac{k_{\mathrm{d}}[M]}{k_{\mathrm{d}}[M] + \bar{k}_{\mathrm{a}}}\right) \times k_{\mathrm{TST}} \tag{54}$$

$$= \kappa^{\mathrm{act}} k_{\mathrm{TST}}$$

where $\bar{k}_{\mathrm{a}}$ denotes the average forward rate constant of the energized molecules and k^{act} means the correction factor due to the collisional activation process. This expression gives the falloff curve which demonstrates the pressure dependence of the unimolecular reaction; the rate increases with increasing pressure and asymptotically approaches the limiting high-pressure value k_{TST}.

On the other hand, the unimolecular reactions in the liquid phase are usually analyzed with the Langevin formalism where the reaction is considered as one-dimensional movement of the reactant along the reaction coordinate.[137,138] In the liquid phase, solvent molecules constantly collide with the reactant molecules and give perturbation throughout the course of the reaction. Such an effect by solvent molecules are considered to be a drag or friction against the barrier crossing. Solvent molecules also exert random force which varies much more quickly than the movement of the reactant along the reaction coordinate. Thus the following Langevin equation expresses the essence of the reaction process in the liquid phase

$$\mu \frac{\partial v}{\partial t} = -\frac{\partial U}{\partial x} - \zeta \mu v + F(t) \tag{55}$$

where μ denotes the reduced mass of the reactant moving along the reaction coordinate x with the velocity v. This equation is a classical Newton's equation and the right-hand side expresses the forces exerted upon the reactant. The first term expresses the external force due to the one-dimensional potential energy curve $U(x)$ along the reaction coordinate, and the second term is the linear dumping term due to the friction which is proportional to the momentum as $-\zeta\mu v$. The third term represents the fluctuating force and $F(t)$ has the following properties where the

$$\langle F(t) \rangle = 0 \tag{56}$$

$$\langle F(t) F(t') \rangle = 2\zeta\mu k_{\mathrm{B}} T \delta(t - t') \tag{57}$$

angle brackets denote the ensemble average.

Kramers solved the above stochastic equation[138] under several assumptions. He assumed $U(x)$ as an asymmetric double-well potential energy surface as shown in Figure 20; the reactant a in a reactant valley proceeds through the potential barrier at *b*

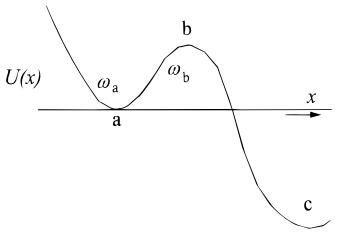

Figure 20. Asymmetric double-well potential energy surface $U(x)$ used in the Kramers theory.

toward the product valley c. The bottom part of the reactant valley can be expressed as

$$U(x) = U(x_a) + {}^1/_2\,\mu\omega_a{}^2(x - x_a)^2 \tag{58}$$

while the barrier at b can be represented as

$$U(x) = U(x_b) - {}^1/_2\,\mu\omega_b{}^2(x - x_b)^2 \tag{59}$$

Since the reaction is considered to proceed along the one-dimensional reaction coordinate, the remaining degrees of freedom for the reactant and solvent molecules are included in the heat bath which as a whole exerts the friction ζ and the random force $F(t)$ on the one-dimensional movement.

By solving the stochastic equation including the random force, Kramers[137,138] derived the rate constant for an unimolecular reaction with a relatively high barrier as

$$k = \left(-\frac{\zeta}{2\omega_b} + \sqrt{1 + \left(\frac{\zeta}{2\omega_b}\right)^2}\right) \times \frac{\omega_b}{2\pi} \exp\left(-\frac{E_a}{k_B T}\right) \tag{60}$$

$$= \kappa^{Kr} k_{TST}$$

where κ^{Kr} denotes the Kramers correction factor to the TST rate. When the crossing region is small and the friction is low, i.e., $(\zeta/\omega_b) \ll 1$, the rate given by eq 60 is reduced to the TST rate. On the other hand, when $(\zeta/\omega_b) \gg 1$, the equation becomes

$$k = \frac{\omega_b}{\zeta} \times \frac{\omega_a}{2\pi} \exp\left(-\frac{E_a}{k_B T}\right) \tag{61}$$

The last equation demonstrates that the rate constant becomes zero at the limit of infinite friction.

Combining above two extremes, the low density limit and the high density−high friction limit, one can imagine the trend in the unimolecular reaction rate with increasing environmental pressure. The rate initially follows the RRKM rate in low-density region and increases with increasing pressure or density toward the maximum value close to k_{TST}. However, at appreciably high pressures, the frictional force begins to work and the rate eventually decreases with increasing pressure/density of the environment as the Kramers theory predicts. That is, collisional activation is replaced by the frictional drag at a certain density. This trend is known as "Kramers turnover". Maneke et al.[139] demonstrated the Kramers turnover in the photoisomerization rate of *trans*-stilbene in gaseous and liquid ethane. Lee et al.[140] also observed the turnover in the same reaction in supercritical ethane. However, both groups found that the absolute value of the reaction rate was much larger than predicted from the Kramers theory.

To improve the Kramers theory, modifications are proposed from several research groups. The central problem here is the evaluation of ζ. In estimating ζ in the Kramers formula, one usually uses the hydrodynamic viscosity η as

$$\zeta = \alpha\pi r\eta/\mu \tag{62}$$

where r is the radius of the rotating moiety. α is the constant expressing the boundary condition, 4 for slip and 6 for stick boundary. It is not taken for granted, however, to apply such macroscopic friction constant to the microscopic interaction between the reactant and the solvent. Lee et al.[141] proposed that ζ in the Kramers equation should be related to the microscopic friction derived from the measured rotational correlation time τ_r through the Hubberd relation,[142] rather than the hydrodynamic η value, as

$$\zeta = \frac{6k_B T}{I}\tau_r \tag{63}$$

where I is the moment of inertia of the twisting group. Such modification improves the fitting to the observed value to some extent.

When a molecule starts rotation, more friction is present in the initial stage than in the steady state. That is, the friction could be time-dependent in contrast to the constant friction assumed in the Kramers theory. On the basis of such considerations, Grote and Hynes[143,144] proposed a theory based on the generalized Langevin equation with the time-dependent friction factor $\zeta(t)$ as

$$\mu\frac{\partial v}{\partial t} = -\frac{\partial U}{\partial x} - \mu\int_0^t \zeta(\tau)v(t-\tau)\,d\tau + F(t) \tag{64}$$

$$\zeta(t) = \frac{1}{\mu k_B T}\langle F(0)F(t)\rangle_{\text{solvents}} \tag{65}$$

Note that the constant friction factor in Kramers formalism can be expressed as

$$\zeta = \int_0^\infty \zeta(t)\,dt \tag{66}$$

According to the Grote−Hynes theory, the unimolecular rate constant can be written as

$$k = \left(-\frac{\zeta(\lambda_r)}{2\omega_b} + \sqrt{1 + \left(\frac{\zeta(\lambda_r)}{2\omega_b}\right)^2}\right) \times \frac{\omega_b}{2\pi} \exp\left(-\frac{E_a}{k_B T}\right)$$

$$= \left(\frac{\lambda_r}{\omega_b}\right) \times k_{TST} \tag{67}$$

$$= \kappa^{GH} k_{TST}$$

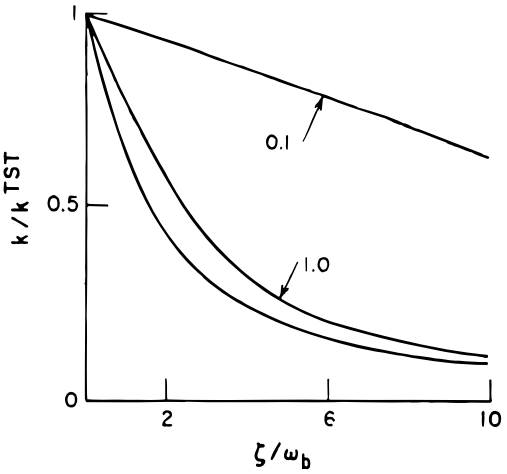

Figure 21. κ^{GH} ($= k/k_{TST}$) value as a function of both ζ/ω_b and the ratio between τ_r and ω_b^{-1}. The numbers in the figure represent the ratio ω_b^{-1}/τ_r. The bottom curve indicates the Kramers limit. (Reprinted with permission from ref 145. Copyright 1985 CRC Press, Inc.)

where $\zeta(\lambda_r)$ is the Laplace transformation frequency component of the friction:

$$\zeta(\lambda_r) = \int_0^\infty e^{-\lambda_r t}\, \zeta(t)\, dt \tag{68}$$

at the reactive frequency λ_r. Although the barrier crossing or reactive frequency is ω_b in the absence of friction, the friction $\zeta(\lambda_r)$ retards the reactive frequency to λ_r. To determine λ_r, one should solve the following self-consistent equation

$$\lambda_r = \omega_b^2[\lambda_r + \zeta(\lambda_r)]^{-1} \tag{69}$$

because the friction itself is the function of λ_r. The ratio of the actual reactive frequency λ_r to the frequency without the friction ω_b then gives the correction factor κ^{GH} to the TST rate as in eq 67.

Since the time correlation $\langle F(0)F(t)\rangle_{solvents}$ is a rapidly decreasing function, it is sufficiently realistic to express $\zeta(t)$ as

$$\zeta(t) = \left(\frac{\zeta}{\tau_r\sqrt{\pi}}\right) \exp\left[-\left(\frac{t}{2\tau_r}\right)^2\right] \tag{70}$$

where τ_r is a molecular relaxation time with the order of 100 fs.[145] Figure 21 shows the κ^{GH} value as a function of (ζ/ω_b) for selected (ω_b^{-1}/τ_r) values. When the barrier crossing time ω_b^{-1} is close to the relaxation time, i.e., $\omega_b^{-1}/\tau_r \cong 1$, large friction is exerted on the reactant motion and therefore the rate approaches to the Kramers limit. On the other hand, when the solvent relaxation time is much longer than the barrier crossing time, i.e., $\omega_b^{-1}/\tau_r \ll 1$, the average friction during the crossing becomes small and the rate approaches to the TST limit. Thus the use of frequency-dependent friction makes the unimolecular rate constant larger than that predicted from the original Kramers theory, and consequently the agreement with the observed rate constant for the rapid barrier crossing reaction is much improved.

It should be noted, however, that since the Langevin equation expresses the one-dimensional diffusion along a hypothetical reaction coordinate separated from other degrees of freedom, the friction constant in the Langevin equation is not necessarily the actual friction but includes all the complicated interactions between the reaction coordinate and other degrees of freedom. One of the promising methods for taking these complexities into account is the molecular dynamics calculation.

2. Experimental Observations in Stilbene Isomerization

trans-Stilbene is a prototype molecule in the study of unimolecular isomerization in gases, liquids, and supercritical fluids. In particular, the isomerization of stilbene in the first excited state was extensively investigated by observing the decay of the fluorescence or the transient absorption of excited *trans*-stilbene. The *trans*-stilbene molecule excited to the S_1 state crosses a small barrier along the reaction coordinate (the twisting angle around the double bond) toward the perpendicular structure which has a deep potential well acting as a funnel to the ground state *cis*- or *trans*-stilbene. The photoisomerization of this prototype molecule is suitable for the RRKM analysis in the gas phase and for the application of the Kramers theory in the liquid phase.

In an isolated molecule limit at cryogenic temperatures, Zewail and co-workers[146,147] measured the photoisomerization rate with picosecond excitation at various excitation energies. They found that at all energies used, the IVR in an isolated stilbene molecule occurred faster than the isomerization, which is the prerequisite for the RRKM analysis. They determined the threshold energy of the reaction to be about 1200 cm^{-1}. They claimed, however, that the isomerization rate derived from the RRKM theory was an order of magnitude larger, and interpreted this discrepancy in terms of the adiabaticity factor at the barrier where diabatic curve crossing might occur. Troe and co-workers[139,148] disagreed with the interpretation and demonstrated that the RRKM theory was able to correctly predict the isomerization rate if the vibrational frequencies at the transition state were appropriately estimated. Recently, Gershinsky and Pollak[149] evaluated the RRKM rate in the gas-phase based on the new potential of Vachev et al.[150] for the isomerization of S_1 stilbene. Using the vibrational frequencies of the reactant and the transition state and the potential barrier height derived from the new potential energy surface, they obtained the energy-dependent gas-phase isomerization rate, which was in good agreement with the measured rate. They also pointed out that the previously observed discrepancy between the observed rate and the RRKM prediction given by the Zewail's group was just an artifact due to the potential energy surface used.

In the liquid phase, on the other hand, the isomerization rate observed is much larger than that predicted by the Kramers theory and even larger than that by the transition state theory.[151] Troe and co-workers[7] considered the reason to be the lowering of the activation barrier by the solvent effect. Since the transition state of the photoisomerization pos-

sesses the zwitterion character due to its electronic structure, the height of the activation barrier must be sensitive to the polarity of the solvent. Even though the solvent is nonpolar, the dispersion interaction could stabilize the polar transition state. As an attempt to include such effect into the Kramers theory, Anderton and Kauffman recently proposed the isodielectric Kramers−Hubbard analysis,[152−154] where the activation barrier is assumed to be a function of the solvent dielectric constant ϵ which in turn is the function of temperature. Although they obtained a reasonable dependence of the activation barrier on ϵ for the isomerization of stilbene in *n*-alcohols, the dependence of ω_a (the frequency of the reactant well) on ϵ appeared unphysical.

Another significant discrepancy between the prediction of the Kramers theory and the observed viscosity dependence of the isomerization rate of *trans*-stilbene in *n*-alkane solvents was reported.[155] Rothenberger et al. adopted the Grote−Hynes modification of the Kramers theory and obtained the better agreement with the observation; however, they used an unphysically low curvature (~8 cm^{-1}) for the potential barrier. Lee et al.,[141] on the other hand, evaluated the microscopic ζ in the Kramers equation from the Hubberd relation, and showed that the Kramers equation predicted the isomerization rate quite well when ζ was evaluated from the rotational correlation time τ_r instead of the viscosity η of *n*-alkane solvents. For further improvement, the multidimensional effect in the barrier crossing should be taken into account since the above theories are based on the one-dimensional diffusion scheme.

For the gas−liquid transition region, Lee et al.[140] determined the photoisomerization rate of *trans*-stilbene in supercritical ethane of 0−170 atm at 350 K by observing the fluorescence decay of S_1 *trans*-stilbene. They reported that the Kramers turnover took place at much higher pressure than the critical pressure. In the plot of isomerization rates against the pressure, they noticed a plateau around the critical pressure. A comment may be necessary to their report. Although they reported the regions of the turnover and the plateau in terms of pressure, it is desirable to describe the regions in terms of density because the density is more directly related to the phenomena occurring in supercritical fluids. When the rate is plotted against the density, the turnover occurs at the density of 0.24 g/cm^3 which is close to the critical density ρ_C, 0.203 g/cm^3. Similarly, the plateau region appears around the density of 0.06 g/cm^3 which is much smaller than ρ_C. They also noticed that the maximum isomerization rate at the turnover region to be much larger than expected from TST and suggested several reasons such as clustering, field effect and high dimensionality of the potential surface.

Maneke et al.[139] measured the photoisomerization rate of *trans*-stilbene in high-pressure gaseous ethane and in liquid ethane under high pressure with picosecond absorption spectroscopy. Their results together with the observation from other groups are summarized in Figure 22, which clearly shows the

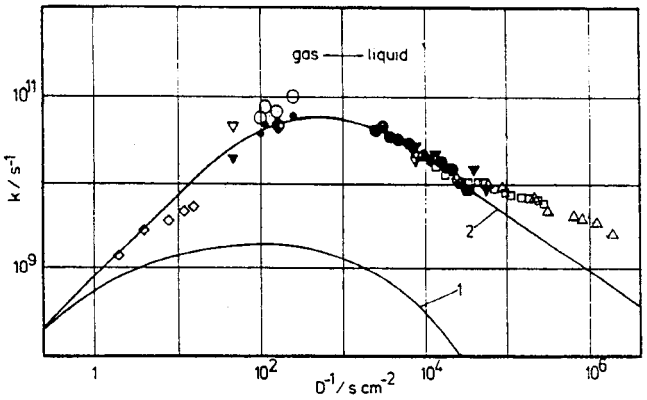

Figure 22. Photoisomerization rate of *trans*-stilbene in high-pressure gaseous ethane and in liquid alkanes under high pressure with picosecond absorption spectroscopy. Symbols indicate the kinds of alkanes used as solvent (see the original paper for details). The line 1 is based on the isolated molecule specific rate constant $k(E)$ and the Kramers model. The line 2 is the prediction from a model which takes into account the cluster- and cage-solvent shifts of the threshold energy E_0. (Reprinted with permission from ref 139. Copyright 1985 Deutsche Bunsen Gesellschaft fur Physikalische Chemie.)

presence of the Kramers turnover. They attempted to fit the data with the extrapolation formula

$$\frac{k}{k_\infty} \approx \frac{C(k_0/k_\infty)}{C[(k_0/k_\infty)+1]+(k_0/k_\infty)^2} \qquad (71)$$

$$C = \frac{k_0}{k_\infty}\frac{k_{diff}}{k_\infty}$$

where k_0 and k_∞ are the low- and high-pressure limit gas-phase rate constants, respectively, calculated from the RRKM theory (note that k_0 includes the bath gas pressure [M]). k_{diff} is the Kramers rate constant at high viscosity limit

$$k_{diff} = \frac{\omega_b}{\zeta} k_\infty \qquad (72)$$

However, the prediction from the above equation was an order of magnitude smaller than the experimental rate as shown in Figure 22 (line 1). To explain the discrepancy, Maneke et al. have proposed the involvement of a stilbene−solvent cluster which lowers the activation barrier, and accelerates the reaction. They considered the equilibrium, $A + M \rightleftharpoons AM$, with an equilibrium constant of K_{cl} and expressed the rate constant as

$$k \approx k_{free}\frac{1}{1+K_{cl}[M]} + k_{cl}\frac{K_{cl}[M]}{1+K_{cl}[M]} \qquad (73)$$

where k in eq 71 is written as k_{free}, and k_{cl} is the same as k except that the activation energy is lowered because of the stabilization by clustering. The line 2 in Figure 22 is obtained by putting K_{cl} to be 10^3 cm^3 mol^{-1} and reducing the activation energy by 800 cm^{-1}. They related the decrease of the barrier height to the solvatochromic shift in the absorption spec-

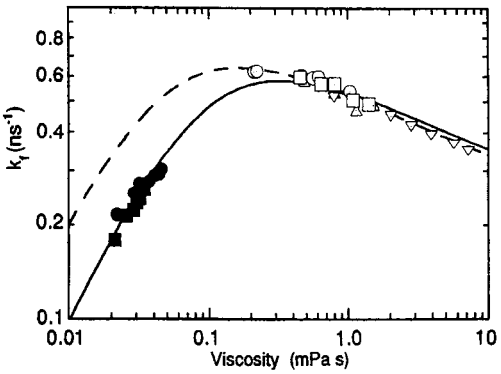

Figure 23. Kramers turnover in the isomerization of 2-vinylanthracene (2VA) studied in supercritical ethane (■), supercritical CO_2 (●) and pressurized *n*-alkanes (pentane ○, hexane □, octane △, and decane ▽). (Reprinted from ref 160. Copyright 1995 American Chemical Society.)

trum. Gehrke et al.[156] observed the similar trend also in the photoisomerization of diphenylbutadiene in supercritical alkanes, CO_2, SF_6, and He.

3. Isomerization around a Single Bond

Isomerization around a single bond has been carried out both in liquids and supercritical fluids to assess the validity of the Kramers theory. In particular, the isomerization of 3,3-diethyloxadicarbocyanine iodide (DODCI) and vinyl anthracene (VA) derivatives has been extensively studied. Veisko et al.[157] measured the viscosity dependence of the DODCI isomerization rate in a series of normal alcohols and concluded that the prediction by the Kramers theory, the linear dependence to the inverse of η, was not satisfied. The modified Kramers theory by Grote and Hynes,[143] which incorporates the frequency-dependent friction, gave a better fit to the observed isomerization rate−viscosity relation. Later, Hara and Akimoto,[158] changing the solvent viscosity over a wider range by means of high-pressure, also demonstrated that the Grote−Hynes theory gave a better fit than the Kramers theory.

Flom et al.[159] proposed another prototype system for isomerization study, 2-vinylanthracene (2VA), and again showed the validity of the frequency-dependent friction formalism. Hara et al.[160,161] studied this system in supercritical ethane and pressurized liquid solvents using picosecond fluorescence decay measurements. They observed the Kramers turnover as shown in Figure 23 and found that the activation energy decreased from the gaslike region to the high viscosity limit by 1.6 kJ/mol. Recently, they[162] conducted a similar experiment with 2-(2-propenyl)-anthracene (22PA) and observed that the rate increases in supercritical region with increasing collision number in line with the energy transfer scheme proposed by Troe's group.[85]

4. The Effect of Clustering on Isomerization Reactions

The clustering in supercritical region seems to affect the isomerization reaction in two ways. One is the enhanced friction against the deformation of molecules such as the twisting motion, and the other is the lowering of the activation barrier with a possible change of the curvature (the imaginary frequency) at the transition state. The use of rotational correlation time τ_r instead of hydrodynamic viscosity η for the evaluation of ζ in the Kramers equation is a promising method for incorporating the effect of microscopic friction due to the clustering. It is desirable, however, to provide a formalism for correlating directly the clustering to the frictional coefficient ζ. A simple way would be the estimation of ζ from the Stokes law with the use of effective $\eta(\rho_{local})$ in place of $\eta(\rho_{bulk})$ as

$$\zeta = \alpha\pi r\eta(\rho_{local})/\mu \qquad (74)$$

where the viscosity is given as a function of ρ, and the local density ρ_{local} is directly related to the clustering.

Concerning the lowering of the barrier height, Hick et al.[163,164] pointed out that the solvent effect on the charge-transfer reaction was not due to the viscosity but the polarity of solvents, and estimated the activation barrier height E_a using a measure of solvent polarity, $E_T(30)$, for individual solvent as

$$E_a = E_a^0 - A[E_T(30) - 30] \text{ (in kcal/mol)} \qquad (75)$$

where A expresses the sensitivity of the relevant reaction to the solvent polarity. This type of modification can be applied for the systematic reduction of the barrier height as a function of clustering number.

F. Electron Transfer and Ionic Reactions

Both intra- and intermolecular electron-transfer reactions cause a dramatic change in the dipole moment of the reacting system. In such reactions, the polar character of the transition state makes the energy and structure of the transition state extremely sensitive to the polarity of the environment. The rate of electron-transfer reactions therefore serves as a sensitive measure of the polar character of supercritical fluid as a function of density.

In ionic reactions, the transition state could be more polar than the initial state in some cases, and in other cases it is less polar. For example, in simple S_N2 reactions, an electronic charge in the transition state expands all over the molecular frame, in contrast to the reactant state where the charge locates on the attacking anion. Electromagnetism teaches us that the more the charge is concentrated, the more it is stabilized in polar solvent. Thus, the activation energies of S_N2 reactions become considerably higher in the more polar solvents. On the other hand, in the heterolysis reaction where the neutral reactant forms a cation and an anion, the transition state is extremely polar because of the separating charges and consequently the activation energy is much lowered in polar solvents.

To discuss the polarity effect on these kinds of reactions one should calculate the degree of stabilization by polar solvent in both the reactant and the transition states. The simple and convenient way is to consider the environment as a continuum with a dielectric constant ϵ, and calculate the stabilization of a dipole or ionic solute molecule in this continuum. However, in supercritical fluids, the clustering occurs

in the immediate vicinity of the polar solute molecule; the actual environment for the solute molecule is not uniform and cannot be approximated as a continuum. A simple modification to incorporate such inhomogeneity is to use the effective dielectric constant instead of the bulk value.

More accurate analysis could be possible if one calculates the electronic state including a central solute and many surrounding solvent molecules using rigorous quantum mechanical formalism. However, even with the high-speed computers available, rigorous time-dependent calculations of a reacting system consisting of a large number of molecules are quite tedious and time-consuming. Therefore, we usually use classical molecular dynamic (MD) calculations where we assume the solvent−solute and solvent−solvent molecular interaction potentials which are either empirical or based on the rigorous molecular orbital calculations. An extensive review on the MD calculations of supercritical water was recently written by Nakahara et al.[165]

1. Theoretical Treatment of the Stabilization of Polar State by Solvents

a. The Onsager's Reaction Field Theory in Continuum Media. The Onsager's reaction field theory[166,167] provides a simple and frequently used formalism to estimate the stabilization energy of a dipolar molecule in polar environment. His model consists of a solute molecule of dipole moment μ in a cavity of radius a formed in a continuum medium whose dielectric constant and reflective index are ϵ and n, respectively. The dipole of the solute molecule generates the electric field which affects the continuum outside the cavity. The polarization of the continuum medium is increased by this electric field and exerts an additional field to the central solute molecule. Such additional field is called "reaction field" and becomes the origin of the stabilization of the solute molecule. According to his calculation, the stabilization energy is given by,

$$\Delta E = \frac{\mu^2}{a^3}\frac{2(\epsilon - 1)}{2\epsilon + 1} \tag{76}$$

Using this equation, one can derive the formula known as the "Lippert−Mataga−Ooshika equation", expressing the absorption spectral shift $\Delta\nu_{abs}$ of a molecule whose dipole moments of S_0 and S_1 states are μ_g and μ_e, respectively, as[168,169]

$$\Delta\nu_{abs} = \frac{\mu_g^2 - \mu_e^2}{a^3}\frac{n^2 - 1}{2n^2 + 1} + \frac{2\mu_g(\mu_g - \mu_e)}{a^3}\left(\frac{\epsilon - 1}{\epsilon + 1} - \frac{n^2 - 1}{n^2 + 2}\right) \tag{77}$$

This equation is often used to estimate the spectral shift in supercritical fluids. If the dipole moment of the transition state is known or calculated, one can also evaluate the stabilization energy of the transition state with eq 76.

b. A Compressible Continuum Model. For considering ionic reactions in supercritical fluids, one has to consider both the simple electrostatic stabilization and the compression of the medium simultaneously during the reaction. Recently, Luo and Tucker proposed a new method,[170] a compressible continuum model. Their idea is that the charge distribution in the solute or reacting molecules produces an electrostatic field $E(r)$ which induces the solvent compression or enhances the solvent density $\rho(E)$ as a function of the field strength. However, since the dielectric constant is a function of the solvent density as $\epsilon(\rho)$ and the electric field is a function of ϵ as $E(\epsilon)$, this compression again changes the electrostatic field. To reach the self-consistent solution of E and ρ, Luo and Tucker solved the Poisson's equation iteratively with the finite-difference grid algorithm.

Using the above method, they calculated the local solvent density of water in the course of anisole hydrolysis reaction[171]

$$PhOCH_3 + OH_2 \rightarrow PhO^- + CH_3OH_2^+$$

They used the Hartree−Fock 6-31G** calculations for obtaining the charge density distribution within the reacting system. They found that even at the low bulk density of 0.25 g/cm^3, the local density of solvent water within 2 Å from the reactant molecule is almost the same as that at 0.5 g/cm^3. In the ordinary continuum model, the free energy of solvation is calculated as the sum of works for carrying the charges in a vacuum together in the medium with the dielectric constant ϵ. In the present model, the charges are carried together through the medium of *varying* dielectric constant and the electronic field $E(r)$. The free energy of solvation was found to be 11.6 kcal/mol lower than the value expected from the ordinary continuum (incompressive) model. They[172] also applied the model to a typical S_N2 reaction

$$Cl^- + CH_3Cl \rightarrow CH_3Cl + Cl^-$$

and compared with the MD calculations.[76,173] As compared with the incompressive model, the compressible continuum model gave much better agreement with the MD calculation in the solvation energy along the reaction path.

The above model seems to be suitable for the ionic reactions in supercritical water whose dielectric constant varies appreciably with the density of water at supercritical temperatures. For reactions in ordinary supercritical fluids, where the density dependence of dielectric constant is not large, the use of ordinary continuum model modified by the effective local density may still be useful for its simplicity.

c. Molecular Dynamics Calculations. With the rapid progress in the fast computer technology, classical molecular dynamic (MD) calculations of a large system consisting of more than 1000 molecules become possible. The calculations dealing with the pure supercritical fluids have been performed for a variety of fluid molecules such as Ar, Xe, CO_2, H_2O, and CF_3H.[3,174] The binary systems consisting of a nonreactive solute molecule and supercritical fluid molecules have been studied with the MD calculations to demonstrate the existence of clusters and characterize them in various fluid conditions.[34−36]

The MD calculations of reacting systems are still very difficult and only a few systems have been treated rigorously. The most primitive way of incorporating the effect of solvent molecules on reaction dynamics is the use of potential of mean force instead of the potential energy surface for an isolated reacting system. Monte Carlo calculations are performed in order to evaluate the potential of mean force by averaging the effects of randomly located solvent molecules on the electronic energy of the reacting molecule. Thus obtained potential of mean force is utilized in combination with the one-dimensional diffusion model such as the Kramers formalism.

A variety of methods have been used for incorporating the effect of solvent molecules into the electronic energy of reacting molecules. With the charge distribution of the reacting system being fixed, one can calculate the Coulombic interaction energies between the charge distribution of the reactant and an ensemble of solvent molecules. One can also explicitly include the effect of solute−solvent interaction into the Hamiltonian of the reacting molecules in SCF-MO calculations. Furthermore, the Hamiltonian of the total system consisting of all the solvent molecules and the reacting molecules could be solved directly by an ab initio SCF-MO method. Although the last method formally gives the most precise results, one needs enormous time on a high-speed computer. Even for a single trajectory, one must solve a time-dependent Hamiltonian equation starting from a reactant pair immersed in solvent molecules with randomly selected initial location to a final product pair all through the reaction path. Nevertheless, theoreticians continuously pursue the new algorithm to shorten the computation time.

The MD calculations are most effective in clarifying the effect of solvent molecules on a rapid reaction occurring with the time scale similar to the fluctuation. Even with the MD calculation of ordinary level, we can extract valuable information on the fluctuation of the environment for reactions, which other methods cannot provide.

2. Intramolecular Charge-Transfer Reactions

When a molecule possesses both electron-donating and electron-accepting parts within a single molecular frame, intramolecular electron transfer may occur on electronic excitation. Hereafter, we call the electron transfer from the donor to the acceptor parts as *charge transfer* in the reverse direction, since the phrase "charge transfer (CT)" has been commonly used for organic donor−acceptor molecules. The efficiency of charge transfer depends on the strength of electron-releasing and electron-withdrawing ability of the component parts, as well as the distance and the orientation between them. When a typical electron donor−acceptor molecule, *N*,*N*-dimethylaminobenzonitrile (DMABN), is photoexcited in polar solvent, anomalously red-shifted emission is observed in addition to the normal fluorescence.[175] The origin of this "anomalous" emission had been a subject of controversy during 1960s and 1970s. Rotkiewicz, Grellmann, and Grabowski have proposed that the emission comes from a charge transfer state where the dimethylamino group twists by 90° from the benzene plane.[176] Although several other suggestions were made,[177,178] the concept of "twisted intramolecular charge transfer (TICT)" state seems to be accepted.

The dipole moment of DMABN in S_0 state is reported to be 7.6 D, whereas in S_1 state it increases to 9.1 D. Further, the dipole moment of the CT state is estimated to be 13 D. With such a dramatic change of the dipole moment in every step, the reorganization of polar solvent molecules should occur simultaneously on charge transfer in the DMABN molecule and this reorganization of solvent may act as the rate-determining step.[179] The rate constants for the charge-transfer reaction of DMABN were determined in a variety of liquid solvents and in some cases the rate was found to be faster than the longitudinal relaxation time of solvents.[180] This variety can be well interpreted by the theory proposed by Sumi and Marcus,[181] which uses the two-dimensional potential surface consisting of the solvent coordinate and the twisting coordinate, instead of the Kramers one-dimensional picture. Although both the solvent reorganization and the twisting of the dimethylamino group are necessary to form the equilibrium charge transfer state, the twisting could occur first to facilitate the electron transfer and then solvent molecules slowly adapt themselves. In this case, the twisting motion controls the CT rate. The feasibility of this motion is determined by the barrier height along the twisting coordinate and the microscopic friction exerted on the motion by the surrounding molecules.

In supercritical fluid, Kajimoto et al.[55,72] first made a systematic analysis of the CT fluorescence of DMABN observed in compressed CF_3H. Using stationary fluorescence spectroscopy, they demonstrated that the CT fluorescence increased rapidly with increasing density of polar fluid molecule CF_3H from 0.025 to 0.7 g cm^3. At the same time they observed the red-shift of the fluorescence maximum with increasing density. The latter observation indicates that the increasing polarity of the environment stabilizes the CT state to diminish the energy between the CT and the ground states. In comparison with the spectral shift estimated from the Lippert−Mataga equation for fluorescence,[169] the observed shift was considerably large at low fluid densities. This fact led the authors to interpret this excess shift of the CT fluorescence in terms of clustering in supercritical fluids. From the plot of the spectral shift against density, the effective local density around the molecule in the CT state could be evaluated at an arbitrary bulk density. The ratio of the integrated CT fluorescence to the S_1 fluorescence, on the other hand, expresses the equilibrium constant of the CT state formation in the excited state, which increases with increasing density.

Kajimoto et al.[70,182] then measured the rate of the CT state formation of DMABN by observing both the decay of the S_1 fluorescence and the rise of the CT fluorescence with picosecond single photon counting technique. They found that the rate of the CT state formation increased with increasing fluid density as

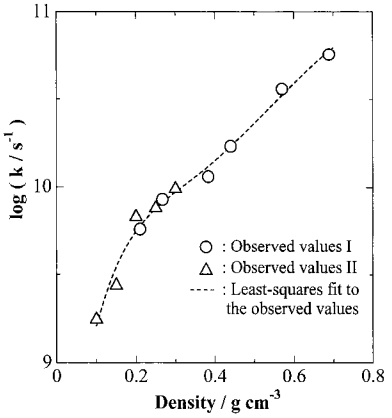

Figure 24. Rate of the CT state formation for DMABN in supercritical CF_3H as a function of fluid density. (Reprinted with permission from ref 70. Copyright 1997 Deutsche Bunsen Gesellschaft fur Physikalische Chemie.)

given in Figure 24. With increasing viscosity, the twisting motion could be slowed and the rate of the reaction may be retarded in liquid phase. However, the stabilization of the transition state due to the increasing environmental polarity is more important in the present reaction and consequently the rate increases with increasing density.

To relate the rate of the CT state formation to the clustering of fluid molecules, they performed an MD simulation of the fluid solvent with a single spherical solute molecule which mimics a DMABN molecule and exerts a large attractive force to the solvent molecules.[70] The computed average clustering number was found to be in excellent parallel to the logarithm of the observed rate constant in their density dependence. This implies that the activation energy of the reaction decreases linearly to the average clustering number n as

$$k = A \exp[-(E_a^0 - n\Delta E)/k_B T]. \qquad (78)$$

According to the MD calculation, the fluctuation of the environment occurs in a time scale of 0.5−2 ps and varies with the fluid density. When the barrier crossing time is much slower than the fluctuation time, the reaction is then considered to proceed on the potential of mean force, averaged over the solvent fluctuation. Such situation probably corresponds to the imaginary frequency of the barrier $\omega_b < 5$ cm^{-1}. On the other hand, when $\omega_b \approx 20$ cm^{-1}, the barrier crossing time becomes comparable to the environmental fluctuation or the fluctuation of the activation barrier, and hence the reaction may seriously affected by the fluctuation.[183] Although, in the CT reaction of DMABN, such effect is not obvious probably due to the slow barrier crossing, the effects of fluctuating polar environment or a fluctuating barrier height must be taken into account in considering rapid reactions in supercritical fluid. This type of fluctuation also provides a challenging problem for the theoretical analysis where the time-independent potential of mean force has been used so far for the barrier crossing problem.

The fluctuation of the polar environment in supercritical fluids is primarily controlled by the *fluctuating number* of the clustering fluid molecules around a solute and its time scale seems to be a few hundred femtoseconds. In contrast, in liquid solvents, the *librational motion* of solvent molecules determine the time scale of the solvent adaptation to the new dipole created in the solution just like the formation of the charge transfer state. Fleming et al. have recently determined the time scale of this process for acetonitrile using the dye molecule LDS-750 to be about 70 fs. [184]

Schulte and Kauffman[185] observed the fluorescence spectra and its decays of bis(4,4′-(dimethylamino)-phenyl)sulfone (DMAPS) in mixed ethanol−CO_2 supercritical fluid solution, and estimated the enrichment of ethanol in the immediate vicinity of the DMAPS molecule to be 5−10 times of the bulk composition. To estimate the effect of clustering on the folding motion, Kauffman and co-workers[186] studied the dynamics of folding in 9-anthryl-$(CH_2)_3$-(4-*N*,*N*-dimethylaniline) and subsequent CT state formation in mixed ethanol−CO_2 supercritical fluid solution.

3. Intermolecular Charge-Transfer Reactions

Takahashi and Johna,[187] using pulse radiolysis technique, examined the density dependence of the intermolecular charge-transfer rate between a biphenyl anion and pyrene in supercritical ethane. The second-order charge transfer rates were found to be nearly constant over the pressure range 55−133 bar. They suggested two possible reasons for this observation, solvent clustering and the dependence of solvent reorganization energy on pressure. Kimura et al.[188] measured an electron-transfer (ET) rate in the hexamethylbenzene−tetracyanoethylene complex in supercritical carbon dioxide. The ET rate was found to increase by almost a factor of 2 on increasing the solvent density from ρ_c to $2\rho_c$. The density dependence was well simulated by the method based on the theory of Marcus[189] and Jortner,[190] although it predicts a somewhat smaller density effect in the higher density region. Recently, Kimura et al.[191] studied the back-electron transfer (b-ET) rate of the same charge transfer complex in various supercritical fluids at 323.2 K. They found that the b-ET rate increased with increasing density of CO_2 and N_2O. On the basis of the Marcus−Jortner theory, they estimated the reaction free energy and the solvent reorganization energy using the absorption spectral shifts. Both parameters showed the stronger density dependence at lower densities than at high densities.

4. Ionic Reactions

Ion−molecule reactions and ion generating reactions have recently been studied in supercritical fluids, particularly in supercritical water. MD simulation of these ionic reactions has also been conducted for supercritical water. The main interest of the studies in supercritical water is the density and temperature dependence of the rate of reactions including charged species, since the dielectric constant ϵ changes dramatically from 78 for ambient condition to 2.6 at the critical temperature (374 °C) and at the density of 0.16 g/cm^3. Also interesting is the solvation of ionic species by water molecules or

water clusters. The local density, and hence local ϵ, of water could be still large even at high temperature and low density because of the strong interaction between the ionic species and water molecules. If this is the case, the ionic reaction may occur easily in the water cluster even at low bulk density. Since supercritical water can dissolve inorganic gases as well as nonpolar organic species, we now acquired an excellent medium where both the ionic and nonpolar species could exist in high concentrations and consequently ion−molecule reactions proceeds quite efficiently.

The general trend in the density dependence of the ionic reactions can be explained from a simple idea of stabilization by solvent in the transition state relative to the reactant state. When the transition state is more polar or possesses concentrated charge distribution than the reactant state, the increase in ϵ lowers the reaction barrier and accelerates the reaction. This is the case in charge generating reactions such as the proton transfer from 2-naphthol to ammonia. On the other hand, when the charge spreads over the reactants in the transition state, the reverse is true as in the case of S_N2 reactions. This type of stabilization most profoundly controls the density and temperature dependence of the ion reactions in supercritical fluid. The stabilization of the polar transition state is then controlled by the local ϵ instead of bulk one; the local ϵ is determined by the clustering under specific density and temperature conditions.

Johnston, Fox, and Rossky at University of Texas at Austin intensively studied the solvation and reactions in supercritical water both experimentally and theoretically. Ryan et al.[192] studied the proton transfer from 2-naphthol to both neutral (NH_3 and H_2O) and anionic species (acetate and borate anions) in supercritical water. For the latter species, they found only modest deviations from Arrhenius-like behavior from ambient temperature to near the critical temperature. In contrast, the rates of proton transfer to ammonia and water exhibited marked deviations from Arrhenius-like behavior and went through the maximum at high temperatures. The loss of local water structure and changes in dielectric constant with temperature exert a profound influence on the charge-generating reactions. At temperatures above 250 °C, contact ion pair formation further inhibits proton transfer. Ryan et al.[193] also observed the acid−base equilibrium of acridine in supercritical water and reported that the exothermic protonation at ambient temperature turned to endothermic at 315 °C due to the decreasing dielectric constant with increasing temperature.

Concerning the S_N2 reactions in supercritical water, the Texas group made an extensive study using molecular dynamics simulations.[76,173] They found that the coordination number of water around Cl^- was almost unaffected as shown in Figure 25 despite the enormous change in the bulk dielectric constant from 78 at ambient condition to about 3 at the critical temperature. This indicates that the stabilization of ionic species by water molecules still works quite efficiently even in supercritical water. The change of

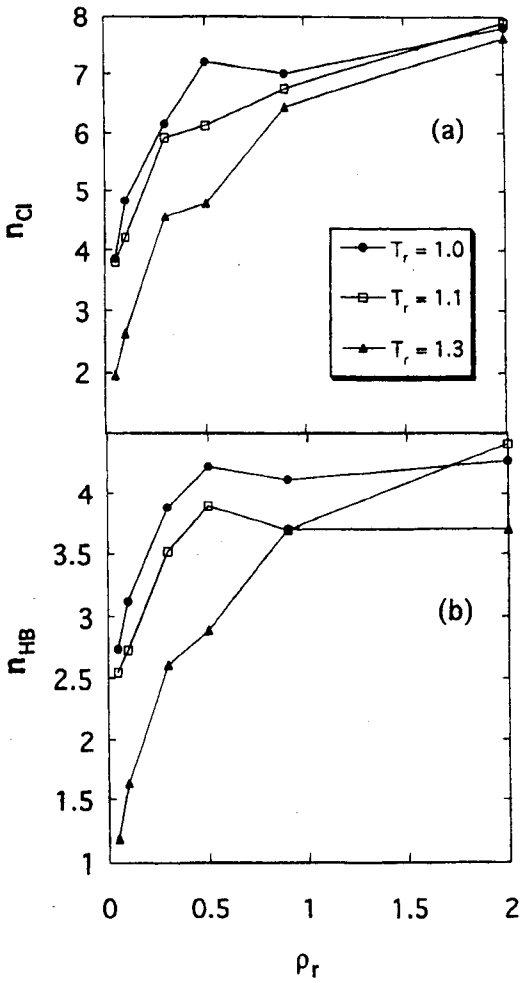

Figure 25. Coordination number of water around Cl^- was almost unaffected even by the enormous change in the bulk dielectric constant from 78 to about 3: (a) coordination number and (b) number of H-bonds of water to Cl^-. (Reprinted from ref 76. Copyright 1995 American Chemical Society.)

the coordination number with density can well be expressed by the Langmuir-type adsorption model, and the enthalpy and free energy changes between the reactant and the transition state can be explained in terms of the variation in average coordination number and hydrogen bonding. They also found that the lifetime of the first solvation shell was about 4 times shorter in supercritical conditions than that in ambient water solution. The useful formalism for the MD calculations of ion reactions in supercritical water is also proposed from other research groups[194,195] and, as a test, both groups treated S_N2 reactions.

The Texas group also examined the ion solvation in supercritical water using the similar MD calculations.[77,196,197] They found that the reduction of the solvation number, during the change of condition from ambient to supercritical, was less in strongly interacting species such as Na^+ and large for weakly interacting neutrals such as HCl. On the basis of the MD simulation results, they proposed a theory predicting the density dependence of the solvation number and solvation free energy, which is a combination of a dielectric concentric shell model and the simple Langmuir-type model of adsorption analogy (see section II.C).

Experimentally, Wallen et al.[198] examined the solvation of water around Br^- in supercritical water using EXAFS measurements and found that the solvation number changed drastically from 7.1 at ambient temperature to 2.8 at 425 °C, whereas at 425 °C it was rather insensitive to the density change of 1.5 times.

Apart from supercritical water, Zhang et al.[199] studied the ion-neutral reaction between arylmethyl cation and tetramethylamine in supercritical CF_3H and C_2H_6 using pulse radiolysis technique. They found that the bimolecular rate constant decreased with increasing density (polarity) probably because of the increase of the activation barrier due to the larger stabilization of the reactant state than that of the transition state.

G. Other Reactions

Other reactions studied in supercritical fluids will be described briefly from the viewpoint of clustering. In some cases, the rate or the equilibrium constant of reactions studied in supercritical fluids were found to have a plateau around the critical density or show an s shape when plotted against the fluid density.

In the dimerization equilibrium of 2-methyl-2-nitrosopropane

$$2\ \textit{tert}\text{-butyl-NO} \rightarrow (\textit{tert}\text{-butyl-NO}-)_2$$

conducted in supercritical CO_2, Kimura et al.[200] found that although the equilibrium constant of dimerization increased with pressure at high-density region, it decreased with pressure/density near the critical density. Such a trend can be understood if one considers the volume change of the dimerization equilibrium. At high densities, the volume of the dimer is less than the two monomers and hence the repulsive compression favors the dimer. However, at medium density where the attractive force helps to form clusters between CO_2 and the reactant, the volume of the initial state (two monomer clusters) are smaller than that of the dimer; the dimerization means the contact of two monomers, which reduces the reactant surface where the CO_2 molecules could be adsorbed. Such reversal of the reaction volume at medium density makes the pressure dependence of the equilibrium opposite in its direction. Thus, the clustering near the critical density plays a crucial role in determining the dimerization equilibria. Kimura and Yoshimura[201] later observed the similar trend in the *rate* of the forward reaction in the same dimerization reaction.

In addition to the volume effect shown above, the density change affects the polarity of the environment as discussed in the preceding two sections. Johnston and Haynes[202] studied the pyrolysis of chlorobenzylmethyl ether in supercritical CH_3CHF_2 and observed more than 2 orders of magnitude increase in the pyrolysis rate as the density of CH_3CHF_2 increased from 0.1 to 1.0 g/cm^3 at 403 K. In the keto−enol isomerization equilibrium of acetylacetone in supercritical CF_3H and CF_3Cl,[203,204] as well as in the tautomerism of 2-hydroxypyridine in CH_3CHF_2,[205] the polar keto form is favored with increasing density.

IV. Future Perspectives

In the present review, we followed the development of the experimental and theoretical researches on the reaction dynamics in supercritical fluids. The central concept in analyzing the behavior of the dynamic processes is solvation or clustering. The main interest of physical chemists in early 1980s was the behavior of collision-induced processes in the gas−liquid transition region. They then became interested in the effect of clusters on the reaction dynamics. The solvent molecules gathering around a reactant molecule could retard the dynamic processes of the reactant by acting as an obstacle to the reactant deformation or the movement. In other cases, the clustering solvent molecules enhanced the polarity in the vicinity of the reactant molecule to facilitate the reactions with polar transition state. The recent interest is extended to the exploration of the effects of environmental inhomogeneity and fluctuations on dynamic processes. Although the effect of the fluctuation on dynamic processes has been a continual theme in physics, no appropriate medium and techniques were available to make the meaningful detection of the effect possible. Supercritical fluids, combined with the developing detection techniques such as ultrashort laser pulses, offer a special opportunity for exploring this theme.

Although the practical applications of the reactions in supercritical fluids were not described in this review, the use of supercritical water as a reaction medium now leads synthetic chemists to new findings of a variety of unexpected reactions in addition to the well-known hydrolysis and oxidation reactions. The mechanism of these new reactions however, still remains to be clarified.

In both the practical and the scientific aspects, "reactions in supercritical fluids" is the extremely interesting and promising gift which this century can offer to the coming century.

V. Acknowledgments

The author thanks Mr. K. Sekiguchi for his critical reading of the manuscript and stimulating discussions. Professor K. Hara and Dr. Y. Yoshimura are also appreciated for their interest and inspiring discussions. Special thanks are due to Mrs. Y. Ueno whose generous help encouraged me to complete this manuscript. This work is partially supported by CREST (Core Research for Evolutional Science and Technology) of Japan Science and Technology Corporation.

VI. References

(1) Andrews, T. *Philos. Trans.* **1869**, *159*, 575−590.
(2) Hannay, J. B.; Hogarth, J. *Proc. R. Soc.* **1879**, *29*, 324.
(3) Hannay, J. B.; Hogarth, J. *Proc. R. Soc.* **1880**, *30*, 178−188.
(4) Villard, P. *J. Phys.* **1894,** *3*, 441−451.
(5) Villard, P. *C. R. Hebd. Seances Acad. Sci.* **1895**, *120*, 182−184.
(6) Michels, A.; Blaisse, B.; Michels, C. *Proc. R. Soc.* **1937**, *A160*, 358−375.
(7) Schroeder, J.; Troe, J. *Annu. Rev. Phys. Chem.* **1987**, *38*, 163−190.

(8) Troe, J. *J. Phys. Chem.* **1986**, *90*, 357−365.
(9) *Supercritical Fluid Science and Technology*, 1st ed.; Johnston, K. P., Penninger, J. M. L., Eds.; American Chemical Society: Washington, DC, 1989; Vol. 406.
(10) *Supercritical Fluid Technology: Theoretical and Applied Approaches in Analytical Chemistry*, 1st ed.; Bright, F. V., McNally, M. E. P., Eds.; American Chemical Society: Washington, DC, 1992; Vol. 488.
(11) *Supercritical Fluid Engineering Science: Fundamentals and Applications*, 1st ed.; Kiran, E., Brennecke, J. F., Eds.; American Chemical Society: Washington, DC, **1992**; Vol. 514.
(12) Savage, P. E.; Gopalan, S.; Mizan, T. I.; Martino, C. J.; Brock, E. E. *AIChE J.* **1995**, *41*, 1723−1778.
(13) Tucker, S. C.; Maddox, M. W. *J. Phys. Chem. B* **1998**, *102*, 2437−2453.
(14) McQuarrie, D. A. *Statistical mechanics*; Harper & Row Publishers: New York, 1973.
(15) Percus, J. K.; Yevick, G. J. *Phys. Rev.* **1958**, *110*, 1.
(16) Stell, G. *Physica* **1963**, *29*, 517.
(17) Frisch, H.; Lobowitz, J. L. *The Equilibrium Theory of Classical Fluids*; Benjamin: New York, 1964.
(18) Wilson, G. M. *J. Am. Chem. Soc.* **1964**, *86*, 127−130.
(19) Mollerup, J. *Fluid Phase Equilib.* **1981**, *7*, 121−138.
(20) Hu, Y.; Ludecke, D.; Prausnitz, J. *Fluid Phase Equilib.* **1984**, *17*, 217−241.
(21) Hu, Y.; Azevedo, E. G.; Prausnitz, J. M. *Fluid Phase Equilib.* **1983**, *13*, 351−360.
(22) Whiting, W. B.; Prausnitz, J. M. *Fluid Phae Equilib.* **1982**, *9*, 119−147.
(23) Johnston, K. P.; Kim, S.; Wong, J. H. *Fluid Phase Equilib.* **1987**, *38*, 39−62.
(24) Nakanishi, K.; Okazaki, S.; Ikari, K.; Higuchi, T.; Tanaka, H. *J. Chem. Phys.* **1982**, *76*, 629−636.
(25) *Faraday Discussions: The equilibrium properties of solutions of nonelectrolyte*; The Royal Society of Chemistry: London, 1953; No. 15.
(26) Robin, S.; Vodar, B. *Discuss. Faraday Soc.* **1953**, *15*, 233−238.
(27) Ewald, A. H.; Jespon, W. B.; Rowlinson, J. S. *Discuss. Faraday Soc.* **1953**, *19*, 238−242.
(28) Franck, E. U. *Z. Phys. Chem. Neue Folge Board* **1956**, *6*, 345−355.
(29) Diepen, G. A. M.; Schefer, F. E. C. *J. Am. Chem. Soc.* **1948**, *70*, 4085−4089.
(30) Diepen, G. A. M.; Schefer, F. E. C. *J. Am. Chem. Soc.* **1953**, *57*, 575−577.
(31) Eckert, C. A.; Zigar, D. H.; Johnston, K. P.; Ellison, T. K. *Fluid Phase Equilib.* **1983**, *14*, 167−175.
(32) Eckert, C. A.; Ziger, D. H.; Johnston, K. P.; Kim, S. *J. Phys. Chem.* **1986**, *90*, 2738−2746.
(33) Kim, S.; Jonnston, K. P. *AIChE J.* **1987**, *33*, 1603−1611.
(34) Petsche, I. B.; Debenedetti, P. G. *J. Chem. Phys.* **1989**, *91*, 7075−7084.
(35) Debenedetti, P. G. *Chem. Eng. Sci.* **1987**, *42*, 2203−2212.
(36) Debenedetti, P. G.; Petsche, I. B.; Mohamed, R. S. *Fluid Phase Equilib.* **1989**, *52*, 347−356.
(37) Economou, I. G.; Donohue, M. D. *AIChE J.* **1990**, *36*, 1920−1928.
(38) Fernandez-Prini, R. *Pure Appl. Chem.* **1995**, *67*, 519−526.
(39) Johnston, K. P.; Kim, S.; Combes, J. In *Supercritical Fluid Science and Technology*, 1st ed.; Johnston, K. P., Penninger, J. M. L., Eds.; American Chemical Society: Washington, DC, 1989.
(40) Hammet, L. P. *Physical Organic Chemistry*, 2nd ed.; McGraw-Hill: New York, 1970.
(41) Grunwald, E.; Winstein, S. *J. Am. Chem. Soc.* **1948**, *70*, 846.
(42) Berson, A.; Hamlet, Z.; Mueller, W. A. *J. Am. Chem. Soc.* **1962**, *84*, 297.
(43) Kosower, E. M. *J. Am. Chem. Soc.* **1958**, *80*, 3253.
(44) Dimroth, K.; Reichardt, C.; Siepmann, T.; Bohlmann, F. *Liebigs Ann. Chem.* **1963**, *661*, 1.
(45) Kamlet, M. J.; Abboud, J. L.; Taft, R. W. *J. Am. Chem. Soc.* **1977**, *99*, 6027−6038.
(46) Kamlet, M. J.; Abboud, J. L.; Taft, R. W. *J. Am. Chem. Soc.* **1977**, *99*, 8325−8327.
(47) Hyatt, J. A. *J. Org. Chem.* **1984**, *49*, 5097.
(48) Sigman, M. E.; Lindley, S. M.; Leffler, J. E. *J. Am. Chem. Soc.* **1985**, *107*, 1471−1472.
(49) Smith, R. D.; Frye, S. L.; Yonker, C. R.; Gale, R. W. *J. Phys. Chem.* **1987**, *91*, 3059−3062.
(50) Yonker, C. R.; Frye, S. L.; Kalkwarf, D. R.; Smith, R. D. *J. Phys. Chem.* **1986**, *90*, 3022−3026.
(51) Kim, S.; Johnston, K. P. *Ind. Eng. Chem. Res.* **1987**, *26*, 1206−1213.
(52) Yonker, C. R.; Smith, R. D. *J. Phys. Chem.* **1988**, *92*, 235−238.
(53) Yonker, C. R.; Smith, R. D. *J. Phys. Chem.* **1988**, *92*, 2374−2378.
(54) Yonker, C. R.; Smith, R. D. *J. Phys. Chem.* **1989**, *93*, 1261−1264.
(55) Kajimoto, O.; Futakami, M.; Kobayashi, T.; Yamasaki, K. *J. Phys. Chem.* **1988**, *92*, 1347−1352.
(56) Sun, Y.-P.; Fox, M. A.; Johnston, K. P. *J. Am. Chem. Soc.* **1992**, *114*, 1187−1194.
(57) Nishikawa, K.; Morita, T. *J. Phys. Chem. B* **1997**, *101*, 1413−1418.
(58) Nishikawa, K.; Takematsu, M. *Chem. Phys. Lett.* **1994**, *226*, 359−363.
(59) Nishikawa, K.; Tanaka, I.; Amemiya, Y. *J. Phys. Chem.* **1996**, *100*, 418−421.
(60) Nishikawa, K.; Morita, T. *J. Supercrit. Fluids* **1998**, in press.
(61) Morita, T.; Nishikawa, K.; Takematsu, M.; Iida, H.; Furutaka, S. *J. Phys. Chem. B* **1997**, *101*, 7158−7162.
(62) Ishii, R.; Okazaki, S.; Okada, I.; Furusaka, M.; Watanabe, N.; Misawa, M.; Fukunaga, T. *Chem. Phys. Lett.* **1995**, *240*, 84−88.
(63) Ishii, R.; Okazaki, S.; Okada, I.; Furusaka, M.; Watanabe, N.; Misawa, M.; Fukunaga, T. *J. Chem. Phys.* **1996**, *105*, 7011−7021.
(64) Ishii, R.; Okazaki, S.; Okada, I.; Furusaka, M.; Watanabe, N.; Misawa, M.; Fukunaga, T. *Mol. Phys.* **1998**, in press.
(65) Chialvo, A. A.; Cummings, P. T. *AIChE J.* **1994**, *40*, 1558−1573.
(66) Munoz, F.; E. H., C. *Fluid Phase Equilib.* **1992**, *71*, 237−272.
(67) Simmons, G. M.; Mason, D. M. *Chem. Eng. Sci.* **1972**, *27*, 89.
(68) Urdahl, R. S.; Rector, K. D.; Myers, D. J.; Davis, P. H.; Fayer, M. D. *J. Chem. Phys.* **1996**, *105*, 8973−8976.
(69) Urdahl, R. S.; Myers, D. J.; Rector, K. D.; Davis, P. H.; Cherayil, B. J.; Fayer, M. D. *J. Chem. Phys.* **1997**, *107*, 3747−3757.
(70) Kajimoto, O.; Sekiguchi, K.; Nayuki, T.; Kobayashi, T. *Ber. Bunsen-Ges. Phys. Chem.* **1997**, *101*, 600−605.
(71) Liew, C. C.; Inomata, H.; Saito, S. *Fluid Phase Equilib.* **1995**, *104*, 317−329.
(72) Kajimoto, O.; Yamasaki, K.; Honma, K. *Faraday Discuss. Chem. Soc.* **1989**, *85*, 65−75.
(73) Bulgarevich, D. S.; Sako, T.; Sugeta, T.; Otake, K.; Uesugi, M.; Kato, M. *J. Chem. Phys.* **1998**, *108*, 3915−3921.
(74) Nakagawa, K.; Otoda, N.; Kimura, A.; Nurdiawati, D.; Tanaka, K.; Kimura, K.; Ejiri, A. *J. Electron. Spectrosc. Relat. Phenom.* **1996**, *78*, 415−418.
(75) Schwarzer, D.; Troe, J.; Zerezke, M. *J. Chem. Phys.* **1997**, *107*, 8380−8390.
(76) Flanagin, L. W.; Baulbuena, P. B.; Johnston, K. P.; Rossky, P. J. *J. Phys. Chem.* **1995**, *99*, 5196−5205.
(77) Flanagin, L. W.; Balbuena, P. B.; Johnston, K. P.; Rossky, P. J. *J. Phys. Chem. B* **1997**, *101*, 7998−8005.
(78) Litovitz, T. A. *J. Chem. Phys.* **1957**, *26*, 469.
(79) Herzfeld, K. F.; Litovitz, T. A. *Absorption and Dispersion of Ultrasonic Waves*; Academic Press: New York, 1959.
(80) Williams, H. T.; Gwynne, V.; Simpson, C. J. S. M. *Chem. Phys. Lett.* **1987**, *136*, 95.
(81) Williams, H. T.; Purvis, M. H.; Simpson, C. J. S. M. *Chem. Phys.* **1987**, *115*, 7.
(82) Chesnoy, J.; Gale, G. M. *Ann. Phys.* **1984**, *9*, 893.
(83) Paige, M. E.; Harris, C. B. *Chem. Phys.* **1990**, *149*, 37.
(84) Harris, C. B.; Smith, D. E.; Russell, D. J. *Chem. Rev.* **1990**, *90*, 481.
(85) Schwarzer, D.; Troe, J.; Votsmeier, M.; Zerezke, M. *J. Chem. Phys.* **1996**, *105*, 3121−3131.
(86) Benzler, J.; Linkersdorfer, S.; Luther, K. *J. Chem. Phys.* **1997**, *106*, 4992−5005.
(87) Tokamakoff, A.; Sauter, B.; Fayer, M. D. *J. Chem. Phys.* **1994**, *100*, 9035.
(88) Oxtoby, D. W. *Adv. Chem. Phys.* **1981**, *47*, 487−519.
(89) Zwabzig, R. *J. Chem. Phys.* **1961**, *34*, 1931−1935.
(90) Cherayil, B. J.; Fayer, M. D. *J. Chem. Phys.* **1997**, *107*, 7642−7650.
(91) Myers, D. J.; Urdahl, R. S.; Cherayil, B. J.; Fayer, M. D. *J. Chem. Phys.* **1997**, *107*, 4741−4748.
(92) Kobayashi, T.; Kajimoto, O. *J. Chem. Phys.* **1987**, *86*, 1118−1125.
(93) Terazima, M. *J. Chem. Phys.* **1996**, *105*, 6587.
(94) Nakabayashi, T.; Okamoto, H.; Tasumi, M. *Private communication*, 1997.
(95) Debye, P. *Polar Molecules*; Dover: New York, 1929.
(96) Einstein, A. *Ann. Phys.* **1906**, *19*, 371.
(97) Stokes, G. *Trans. Cambridge Philos. Soc.* **1956**, *9*, 5.
(98) Youngren, G. K.; Acrivos, A. *J. Chem. Phys.* **1975**, *63*, 3846.
(99) Hu, C. M.; Zwanzig, R. *J. Chem. Phys.* **1974**, *60*, 4354−4357.
(100) Dote, J. L.; Kivelson, D.; Schwartz, R. N. *J. Phys. Chem.* **1981**, *85*, 2169−2180.
(101) Roy, M.; Doraiswamy, S. *J. Chem. Phys.* **1993**, 3213−3223.
(102) Anderton, R. M.; Kauffman, J. F. **1994**, *98*, 12117−12124.
(103) Heitz, M. P.; Maroncelli, M. *J. Phys. Chem. A* **1997**, *101*, 5852−5868.
(104) Jonas, J. *Acc. Chem. Res.* **1984**, *17*, 74−81.
(105) Wakai, C.; Nakahara, M. *J. Chem. Phys.* **1995**, *103*, 2025−2033.
(106) deGrazia, J. L.; Randolph, T. W.; O'Brien, J. A. *J. Phys. Chem. A* **1998**, *102*, 1674−1681.
(107) Anderton, R. M.; Kauffman, J. F. *J. Phys. Chem.* **1995**, *99*, 13759−13762.
(108) Heitz, M. P.; Bright, F. V. *J. Phys. Chem.* **1996**, *100*, 6889−6897.
(109) Hippler, H.; Schubert, V.; Troe, J. *J. Chem. Phys.* **1984**, *81*, 3931.
(110) Otto, B.; Schroeder, J.; Troe, J. *J. Chem. Phys.* **1984**, *81*, 202.
(111) Hippler, H.; Schubert, V.; Troe, J. *Ber. Bunsen-Ges. Phys. Cem.* **1985**, *89*, 760−763.

(112) Brennecke, J. F. *Book of Abstracts*, 215th National Meeting of the American Chemical Society, Spring, Dallas, TX; American Chemical Society: Washington, DC, 1998.
(113) Brennecke, J. F.; Tomasko, D. L.; Eckert, C. A. *J. Phys. Chem.* **1990**, *94*, 7692−7700.
(114) Zagrobelny, J.; Betts, T. A.; Bright, F. V. *J. Am. Chem. Soc.* **1992**, *114*, 5249−5259.
(115) Zagrobelny, J.; Bright, F. V. *J. Am. Chem. Soc.* **1992**, *114*, 7821−7826.
(116) Randolph, T. W.; Carlier, C. *J. Phys. Chem.* **1992**, *96*, 5146−5151.
(117) Jossi, J. A.; Stiel, L. I.; Thodes, G. *AIChE J.* **1962**, *8*, 59.
(118) Batchelor, S. N. *J. Phys. Chem. B* **1998**, *102*, 615−619.
(119) Birks, J. B. *Photophys. Org. Mol.* **1970**, 372.
(120) Yekta, A.; Turro, N. J. *J. Mol. Photochem.* **1972**, *3*, 307−322.
(121) Roberts, C. B.; Zhang, J.; Chateauneuf, J. E.; Brennecke, J. F. *J. Am. Chem. Soc.* **1993**, *115*, 9576−9582.
(122) Roberts, C. B.; Zhang, J.; Brennecke, J. F.; Chateauneuf, J. E. *J. Phys. Chem.* **1993**, *97*, 5618−5623.
(123) Dutoit, J. C.; Zellweger, J. M.; van den Bergh, H. *J. Chem. Phys.* **1983**, *78*, 1825.
(124) Honma, K.; Kajimoto, O. *J. Chem. Phys.* **1987**, *86*, 5491−5499.
(125) Harris, A. L.; Brown, J. K.; Harris, C. B. *Annu. Rev. Phys. Chem.* **1988**, *39*, 341−366.
(126) Vorsa, V.; Paul J.; Campagnola, P. C.; Sreela Nandi, S.; Mats Larsson, M.; Lineberger, W. C. *J. Chem. Phys.* **1996**, *105*, 2298−2308.
(127) Vorsa, V.; Nandi, S.; Campagnola, P. J.; Larsson, M.; Lineberger, W. C. *J. Chem. Phys.* **1997**, *106*, 1402−1410.
(128) Alexander, M. L.; Levinger, N. E.; Johnson, M. A.; Ray, D.; Lineberger, W. C. *J. Chem. Phys.* **1998**, *88*, 6200−6210.
(129) Nadal, M. E.; Kleiber, P. D.; Lineberger, W. C. *J. Chem. Phys.* **1996**, *105*, 504−514.
(130) Lienau, C.; Zewail, A. H. *Chem. Phys. Lett.* **1994**, *222*, 224−232.
(131) Liu, Q.; Wan, C.; Zewail, A. H. *J. Chem. Phys.* **1996**, *105*, 5294−5297.
(132) Lienau, C.; Zewail, A. H. *J. Phys. Chem.* **1996**, *100*, 18629−18649.
(133) Materny, A.; Lienau, C.; Zewail, A. H. *J. Phys. Chem.* **1996**, *100*, 18650−18665.
(134) Eyring, H. *J. Chem. Phys.* **1935**, *3*, 107.
(135) Glasstone, S.; Laidler, K. J.; Eyring, H. *The Theory of Rate Process*; McGraw-Hill: New York, 1941.
(136) Holbrook, K. A.; Pilling, M. J.; Robertson, S. H. *Unimolecular Reactions*; 2nd ed.; John Wiley & Sons: New York, 1996.
(137) Billing, G. D.; Mikkelsen, K. V. *Introduction to Molecular Dynamics and Chemical Kinetics*; Wiley-Interscience: New York, 1996.
(138) Kramers, H. A. *Physica* **1940**, *7*, 284.
(139) Maneke, G.; Schroeder, J.; Troe, J.; Vob, F. *Ber. Bunsen-Ges., Phys. Chem.* **1985**, *89*, 896−906.
(140) Lee, M.; Moltom, G. R.; Hochstrasser, R. M. *Chem. Phys. Lett.* **1985**, *118*, 359−363.
(141) Lee, M.; Bain, A. J.; McCarthy, P. J.; Haseltine, J. N.; Smith, A. B., III; Hochstrasser, M. *J. Chem. Phys.* **1986**, *85*, 4341−4347.
(142) Hubberd, P. S. *Phys. Rev.* **1963**, *131*, 1155.
(143) Grote, R. F.; Hynes, J. T. *J. Chem. Phys.* **1980**, *73*, 2715−2731.
(144) Grote, R. F.; van der Zwan, G.; Hynes, J. T. *J. Phys. Chem.* **1984**, *88*, 4767.
(145) Hynes, J. T. In *Theory of Chemical Reaction Dynamics*; Baer, M., Ed.; CRC Press: Boca Raton, 1985; Vol. 4.
(146) Felker, P. M.; Zewail, A. H. *J. Phys. Chem.* **1985**, *89*, 5402−5411.
(147) Syage, J. A.; Felker, P. M.; Zewail, A. H. *J. Chem. Phys.* **1984**, *81*, 4706−4723.
(148) Schroeder, J.; Troe, J. *J. Phys. Chem.* **1989**, *90*, 4215−4216.
(149) Gershinsky, G.; Pollak, E. *J. Chem. Phys.* **1997**, *107*, 812−824.
(150) Vachev, V. D.; Frederick, J. H.; Grishanin, B. A.; Zadkov, V. N.; Kroteev, N. I. *J. Chem. Phys.* **1995**, *99*, 5247.
(151) Balk, M. W.; Fleming, G. R. *J. Phys. Chem.* **1986**, *90*, 3975−3983.
(152) Anderton, R. M.; Kauffman, J. F. *J. Phys. Chem.* **1994**, *98*, 12125−12132.
(153) Anderton, R. M.; Kauffman, J. F. *Chem. Phys. Lett.* **1995**, *237*, 145−151.
(154) Anderton, R. M.; Kauffman, J. F. *J. Phys. Chem.* **1995**, *99*, 14682−14631.
(155) Rothenberger, G.; Negus, D. K.; Hochstrasser, R. M. *J. Chem. Phys.* **1983**, *79*, 5360−5367.
(156) Gehrke, C.; Schroeder, J.; Schwarzer, D.; Troe, J.; Vob, F. *J. Chem. Phys.* **1990**, *92*, 4805−4816.
(157) Velsko, S. P.; Waldeck, D. H.; Fleming, G. R. *J. Chem. Phys.* **1983**, *78*, 249−258.
(158) Hara, K.; Akimoto, S. *J. Phys. Chem.* **1991**, *95*, 5811−5814.
(159) Flom, S. R.; Brearley, A. M.; Kahlow, M. A.; Nagarajan, V.; Barbara, P. F. *J. Chem. Phys.* **1985**, *83*, 1993−1995.
(160) Hara, K.; Kiyotani, H.; Kajimoto, O. *J. Chem. Phys.* **1995**, *103*, 5548−5553.
(161) Hara, K.; Ito, N.; Kajimoto, O. *J. Phys. Chem. A* **1997**, *101*, 2240−2244.
(162) Ito, N.; Hara, K.; Kajimoto, O. *Submitted for publication*, 1998.
(163) Hicks, J.; Vandersall, M.; Sitzmann, E. V.; Eisenthal, K. B. *Chem. Phys. Lett.* **1987**, *135*, 413−420.
(164) Hicks, J.; Vandersall, M.; Babarogic, Z.; Eisenthal, K. B. *Chem. Phys. Lett.* **1985**, *116*, 118−124.
(165) Nakahara, M.; Yamaguchi, T.; Ohtaki, H. *Recent. Res. Dev. Phys. Chem.* **1997**, *1*, 17−49.
(166) Onsager, L. *J. Am. Chem. Soc.* **1936**, *58*, 1486.
(167) Wilson, J. N. *Chem. Rev.* **1939**, *25*, 377.
(168) Ooshika, Y. *J. Phys. Soc. Jpn.* **1954**, *9*, 594−602.
(169) Mataga, N.; Kubota, T. *Molecular Interactions and Electronic Spectra*; Marcel Dekker: New York, 1970.
(170) Luo, H.; Tucker, S. C. *J. Phys. Chem.* **1996**, *100*, 11165−11174.
(171) Klein, M. T.; Mentha, Y. G.; Torry, L. A. *Ind. Eng. Chem. Res* **1992**, *31*, 182.
(172) Luo, H.; Tucker, S. C. *J. Phys. Chem. B* **1997**, *101*, 1063−1071.
(173) Baulbuena, P. B.; Johnston, K. P.; Rossky, P. J. *J. Am. Chem. Soc.* **1994**, *116*, 2689−2690.
(174) Okazaki, S.; Matsumoto, M.; Okada, I.; Maeda, K.; Kataoka, Y. *J. Chem. Phys.* **1995**, *103*, 8594−8601.
(175) Lippert, E.; Luder, W.; Boos, H. *Advanced Molecular Spectroscopy*; Pergamon Press: Oxford, 1962.
(176) Rotkiewicz, K.; Grellmann, K. H.; Grabowski, Z. R. *Chem. Phys. Lett.* **1973**, *19*, 315−318.
(177) Visser, R. J.; Varma, C. A. G. O.; Konijnenberg, J.; Bergwerf, P. *J. Chem. Soc., Faraday Trans. 2* **1983**, *79*, 347.
(178) Kosower, E. M.; Dodiuk, H. *J. Am. Chem. Soc.* **1976**, *98*, 924.
(179) Kosower, E. M.; Huppert, D. *Chem. Phys. Lett.* **1993**, *96*, 433−435.
(180) Su, S.-G.; Simon, J. D. *J. Chem. Phys.* **1988**, *89*, 908−919.
(181) Sumi, H.; Marcus, R. A. *J. Chem. Phys.* **1986**, *84*, 4894−4914.
(182) Kajimoto, O.; Nayuki, T.; Kobayashi, T. *Chem. Phys. Lett.* **1993**, *209*, 357−360.
(183) Fulinski, A. *Phys. Lett. A* **1993**, *180*, 94.
(184) Resenthal, S. J.; Xie, X.; Du, M.; Fleming, G. R. *J. Chem. Phys.* **1991**, 95, 4715−4718.
(185) Schulte, R. D.; Kauffman, J. F. *Appl. Spectrosc. (USA)* **1995**, *49*, 31−39.
(186) Khajehpour, M.; Greever, J.; Kauffman, J. F. *Book of Abstracts*, 215th National Meeting of the American Chemical Society, Spring, Dallas, TX; American Chemical Society: Washington, DC, 1998.
(187) Takahashi, K.; Jonah, C. D. *Chem. Phys. Lett.* **1997**, *264*, 297−302.
(188) Kimura, Y.; Takebayashi, Y.; Hirota, N. *Chem. Phys. Lett.* **1996**, *257*, 429−433.
(189) Marcus, R. A.; Sutin, N. *Biochim. Biophys. Acta* **1986**, *811*, 265.
(190) Jortner, J. *J. Chem. Phys.* **1976**, *64*, 4860.
(191) Kimura, Y.; Takebayashi, Y.; Hirota, N. *J. Chem. Phys.* **1998**, *108*, 1485−1498.
(192) Ryan, T. R.; Xiang, T.; Johnston, K. P.; Fox, M. A. *J. Phys. Chem.* **1996**, *100*, 9395−9402.
(193) Ryan, E. T.; Xiang, T.; Johnston, K. P.; Fox, M. A. *J. Phys. Chem. A* **1997**, *101*, 1827−1835.
(194) Pomelli, C. S.; Tomasi, J. *J. Phys. Chem. A* **1997**, *101*, 3561−3568.
(195) Ruiz-Lopez, M. F.; Rinaldi, D.; Bertran, J. *J. Chem. Phys.* **1995**, *103*, 9249−9260.
(196) Baulbuena, P. B.; Johnston, K. P.; Rossky, P. J. *J. Phys. Chem.* **1996**, *100*, 2706−2715.
(197) Baulbuena, P. B.; Johnston, K. P.; Rossky, P. J. *J. Phys. Chem.* **1996**, *100*, 2716−2722.
(198) Wallen, S. L.; Palmer, B. J.; Pfund, D. M.; Fulton, J. L.; Newville, M.; Ma, Y.; Stern, E. A. *J. Phys. Chem. A.* **1997**, *101*, 9632−9640.
(199) Zhang, J.; Connery, K. A.; Brennecke, J. F.; Chateauneuf, J. E. *J. Phys. Chem.* **1996**, *100*, 12394−12402.
(200) Kimura, Y.; Yoshimura, Y.; Nakahara, M. *Chem. Lett.* **1988**, 39−42.
(201) Kimura, Y.; Yoshimura, Y. *Ber. Bunsen-Ges. Phys. Chem.* **1993**, *97*, 29−32.
(202) Johnston, K. P.; Haynes, C. *AIChE J.* **1987**, *33*, 2017.
(203) Yamasaki, K.; Kajimoto, O. *Chem. Phys. Lett.* **1990**, *172*, 271−274.
(204) Akao, K.; Yoshimura, Y. *J. Chem. Phys.* **1991**, *94*, 6243−5244.
(205) Peck, D. G.; Mehta, A. J.; Johnston, K. P. *J. Phys. Chem.* **1989**, *93*, 4297.

CR970031L